Spring 1-1-2013

Estimating Ocean Currents from Automatic Identification System Based Ship Drift Measurements

Thomas Dominic Jakub
University of Colorado at Boulder, tjakub@gmail.com

Estimating Ocean Currents from Automatic Identification System Based Ship Drift Measurements

by

Thomas D. Jakub

B.S., The Pennsylvania State University, 2003

M.S., University of Colorado, 2006

A thesis submitted to the

Faculty of the Graduate School of the

University of Colorado in partial fulfillment

of the requirements for the degree of

Doctor of Philosophy

Department of Aerospace Engineering Sciences

2013

This thesis entitled:
Estimating Ocean Currents from Automatic Identification System Based Ship Drift Measurements
written by Thomas D. Jakub
has been approved for the Department of Aerospace Engineering Sciences

Robert Leben

William Emery

Karl Gustafson

Weiqing Han

Jack Harlan

Date

The final copy of this thesis has been examined by the signatories, and we find that both the content and the form meet acceptable presentation standards of scholarly work in the above mentioned discipline.

Jakub, Thomas D. (Ph.D, Aerospace Engineering Sciences)

Estimating Ocean Currents from Automatic Identification System Based Ship Drift Measurements

Thesis directed by Prof. Robert Leben

Abstract:

Ship drift is a technique that has been used over the last century and a half to estimate ocean currents. Several of the shortcomings of the ship drift technique include obtaining the data from multiple ships, the time delay in getting those ship positions to a data center for processing and the limited resolution based on the amount of time between position measurements. These shortcomings can be overcome through the use of the Automatic Identification System (AIS). AIS enables more precise ocean current estimates, the option of finer resolution and more timely estimates.

In this work, a demonstration of the use of AIS to compute ocean currents is performed. A corresponding error and sensitivity analysis is performed to help identify under which conditions errors will be smaller. A case study in San Francisco Bay with constant AIS message updates was compared against high frequency radar and demonstrated ocean current magnitude residuals of 19 cm/s for ship tracks in a high signal to noise environment. These ship tracks were only minutes long compared to the normally 12 to 24 hour ship tracks. The Gulf of Mexico case study demonstrated the ability to estimate ocean currents over longer baselines and identified the dependency of the estimates on the accuracy of time measurements. Ultimately, AIS measurements when combined with ship drift can provide another method of estimating ocean currents, particularly when other measurements techniques are not available.

Dedication

To family and friends, for all the support, advice and time given over the years. In a special way, Heather and Thomas.

Acknowledgements

I would like to thank my committee for providing their time, useful insights and access to data that would otherwise be harder to access.

I would like to thank several groups for the use of their data. Cloudview Photography provided the AIS measurements via their ftp site for San Francisco Bay. Jim Pettigrew and Jack Harlan along with San Francisco State University provided the high frequency radar data for San Francisco. I would like to thank ORBCOMM for providing AIS messages from their satellites for the Gulf of Mexico. I would also like to thank the consortium of institutions that support the HYCOM model.

I would like to thank the numerous colleagues at work for constantly asking if I had finished my dissertation yet. While too numerous to actually name, I do appreciate all the encouragement.

Last, I would like to thank my family. Heather and Thomas for their patience as I wrote and my parents for periodic proofreading.

Contents

Chapter

List of Tables

Table

List of Figures

Figure

Chapter 1

Background

Ship drift is a technique that has been used for over a century and a half to measure ocean currents. Like all ocean current measurement techniques, each process has its own shortcomings. Individual ship drift measurements are normally averaged over large distances for numerous ships to provide a more accurate assessment of the ocean currents. Due to the need to acquire individual ship measurements from multiple ships, a delay in when the data is available also occurs. The Automatic Identification System (AIS) provides a structure to reduce the delay in combining multiple ship records and improving the precision of the ship drift measurements of ocean currents by an order of magnitude compared to ship drift measurements taken within the last 20 years. When combined with satellites, such as ORBCOMM, that can relay these messages back to shore, ocean currents from ship drift measurements can be routinely estimated in a timely manner, to more precision and with global coverage.

The Automatic Identification System (AIS) is an internationally mandated safety of life system for all ships once they reach a certain class. This system provides a large amount of information about how a particular ship is operating at a given instant in time including position, speed, heading and course over ground. The US Coast Guard is investigating ways of getting this ship information further out from the shore than the original 25 nautical miles that the system was designed for [*Tetreault*, 2002]. This new data source has the potential of being used with ship drift techniques to provide ocean surface current measurements. While other in situ measurement techniques such as high frequency radar can measure ocean surface currents, they are limited to

being closer to the shore.

This dissertation focuses on an error analysis and sensitivity analysis of ocean currents as well as their application in two separate case studies. A process is shown as to how to use the AIS measurements to compute ship drifts. Based on the resolution of the AIS messages, an error propagation analysis is performed to determine the precision of the ocean current estimates. A sensitivity analysis is performed to see what parameters the ship drift technique is most sensitive to. A case study is then performed in San Francisco Bay due to the availability of AIS data, high frequency radar data, high ship volume and known ocean currents. A comparison of AIS based ship drift estimates of ocean currents is compared against high frequency radar measurements over the same time period for this case study. A second case study is performed in the Gulf of Mexico using AIS data provided by ORBCOMM to compute ocean current and compares these estimates against both the geostrophic current and the HYCOM model. A quick analysis also demonstrates the ability to use AIS measurements to determine when the ocean currents transitioned using anchored ships that were allowed to freely rotate. Ultimately, the combination of AIS and ship drift provides an inexpensive method of determining ocean current surface currents for globally distributed ship locations.

Chapter 2

Literature Review

Understanding the activities that occur near the coastline are important for economic, environmental, and security related matters. This has contributed to an increase in the number of high frequency radar sites and an increase in AIS monitoring. Although much of this work has focused on ship monitoring or direct ocean currents measurement [*Laws et al.*, 2011][*Vesecky et al.*, 2009][*Vesecky et al.*, 2010], it is possible to characterize ocean currents where direct ocean current measurements are not made. Ship drift from AIS measurements in regions where high frequency radar measurements are not available, provide an additional level of insight into ocean currents.

2.1 Ocean Surface Currents

For this discussion, the ocean surface currents discussed will be in the upper 10s of meters of the ocean. These ocean surface currents are caused by wind driven, inertial and tidal effects [*Pond and Pickard*, 2003]. The wind usually is the dominant force in the open ocean while in shallower water, such as bays and near the coastline, tides can dominate. The ocean currents can vary from barely moving at all to 8 m/s depending on the dynamics of the situation [*Pond and Pickard*, 2003].

Numerous studies on ocean surface currents have been undertaken for a variety of topics. These currents, due to their ability to transport floating matter, have ecological implications as well as pollutant transportation implications in the event of oil spill [*Barrick et al.*, 1977]. Surface currents also impact search and rescue operations for person in the water activities [*Davidson et al.*, 2009]. Ocean currents are also studied for modeling purposes for climate studies [*Deser and*

Blackmon, 1993].

Two approaches are generally used when describing ocean currents, the Eulerian approach and the Lagrangian approach [*Pickard and Emery*, 1990]. In the Eulerian approach, the current′s speed and direction is stated for a specific location. An example of this would be a moored current meter that reports at predetermined intervals. With the Lagrangian approach, the current is described as a function of time along the path of the current. An example of this would be a drifting buoy whose position at subsequent times is used to determine the direction of the current. A similar Lagrangian process was used by *Kim and Terrill* [2009] to observe how oil spills progressed over time.

Several different methods of measuring currents exist including ship drift, drifting buoys, moored current meters, high frequency radar, and other additional methods. Ship drift and drifting buoys both follow the Lagrangian approach in that they describe the ocean current at a specific time and at the next instant in time they will be at a different location. This limits their application for some projects since subsequent to the initial release the next measurement location is not predetermined. Moored current meters, and high frequency radar can describe ocean currents for a specific location over multiple instances of time. Each of the above stated techniques has their advantages and disadvantages and each measures the currents slightly differently. *Pickard and Emery* [1990] provides a detailed history of many of these techniques.

2.2 Measuring Ocean Surface Currents

2.2.1 Ship Drift

Surface currents impart forces on ships. These forces are transmitted to the portion of the ship′s hull below the waterline. The larger the area underwater, the larger the force the ship experiences. Forces from the ocean current deflect ships from their intended courses. While this can be compensated for by navigation techniques it can also provide a measure of the ocean current perturbing the ship. In the mid-1800s, Matthew Fontaine Maury using ship logs produced currents

maps to speed the travels of later ship captains [*Richardson*, 1985]. The technique that he used was ship drift.

Ship drift is a technique that calculates the distance a ship is displaced from its intended course and determines the magnitude and direction of the ocean surface current that displaced the ship. As stated by *Richardson* [1997], a ship drift measurement of surface current is obtained by subtracting the velocity vector between two measured ship position fixes from the estimated dead reckoning velocity vector over the same interval of time. This leads to an easy calculation to make, however the noise associated with the computation requires averaging to get measurements of sufficient accuarcy.

The ship drift dataset has been built upon and used in numerous other investigations including studies of major ocean currents, energetic eddies, and evaluating model simulations [*Richardson*, 1989; *Wyrtki et al.*, 1976]. *Richardson and McKee* [1984] examined ship drifts in the equatorial Atlantic and were able to measure an annual current cycle of 20 cm/s. *Sturges* [1993] successfully used ship drift data to help characterize the western boundary current in the Gulf of Mexico. One major concern pertaining to ship drift measurements is the "windage" effect on perturbing the ocean current measurement. *McPhaden et al.* [1991] determined an upper bound of 3% wind speed, but ultimately relied more on drifter and current meter measurements. *Arnault* [1987] ignored the "windage" effect and was still able to reproduce the seasonal variation of the Atlantic that was under investigation. *Richardson* [1997] investigated this leeway effect and concluded the impact was small. The wave effect is another example of an external force that may distort the estimated ocean current when using ship drift.

2.2.2 High Frequency Radar

Barrick et al. [1977] and *Stewart and Joy* [1974] provide a description of how high frequency radar can directly measure the ocean current near the surface. This direct measurement of a surface current is achieved by transmitting a radar signal (3 to 30 MHz) and examining the returned signal. The transmitted radar signal incurs a Bragg scattering effect on the ocean surface. Therefore, when

this signal is detected by the receiving antenna, if there is no current, two symmetrically spaced peaks about the carrier frequency will be seen. If a current does exist, these peaks will be shifted by the doppler effect. *Barrick et al.* [1977] has an excellent graphic that illustrates this phenomenon.

A practical consideration when selecting a high frequency radar system includes how the wavelength at which the system operates should be chosen based on the local wave conditions. Ideally, the ocean waves should be a 1/2 of the wavelength of the transmitted signal to maximize the first order Bragg scattering effect [*Barrick et al.*, 1977]. A range to the current can be computed by modulating a chirp on the transmitted signal. The direction of the transmitted signal can be varied either through the use of a phased array or a synthetic aperture [*Calvin C Teague and Fernandez*, 1997]. By varying the range and direction of the transmitted signals, a current map of a region can be created. These transmitted signals produce a measure of current in a radial direction from the high frequency radar site. When these individual radial files are combined for multiple sites, a total vector file can be created that shows the currents in a non-site specific reference frame.

One additional note about high frequency radars is due to the frequencies involved, the transmission and receiving antennas are often in different locations. More recently, *Paduan et al.* [2006], demonstrated that by calibrating the receive antenna of the high frequency radars, smaller bearing errors are achieved with the radial measurements. Paduan estimated a radar velocity error of 6.9 - 9.2 cm/s. Another error source demostrated by *Ohlmann et al.* [2007] was a sampling error due to the difference in resolution between the HF Radars and the high resolution drifter data. This error source was estimated to be approximately 5 cm/s.

2.2.3 Tidal Predictions

In coastal regions where the currents are dominated by the tides, the time of the currents can be determined from tidal models. As the tides can be predicted from harmonic analysis of the sun and the moon, the maximum currents can also be predicted. One relationship between the tidal currents and the tides themselves is they are out of phase with each other [*Pond and Pickard*, 2003]. At the maximum high tide, there is a slack current, ie. no water movement. Between the

high tide and the low tide, the ebb current will be at its maximum. This allows, for regions where no direct current measurement is available, tidal predictions to be used to determine what type of ocean current is occurring.

2.2.4 Other Current Measuring Techniques

While this list is not inclusive of every method of measuring ocean currents, it is intended to provide additional insight into techniques that have been shown to be able to measure ocean currents. *Leben et al.* [2002] has demonstrated the use of satellite altimetry to measure mesoscale ocean currents. Synthetic Aperture Radar has also been shown to work in areas with strong current gradients and the need to measure a large area [*Graber et al.*, 1996]. Sea surface temperature can also be used to determine ocean currents.

2.2.5 Comparison of Techniques

There have been numerous studies examining how well one method of ocean current computation compares to other observation methods. *Emery et al.* [2004] and *Barrick and Rector* [2011] are examples where high frequency radar has been compared against current meters. Current meters and high frequency radar measure the currents differently, and consequently do have slightly different measured current values. Current meters can be moored, but this is often done at a depth rather than the surface itself. This reduces the wave and wind effects on the moored meters. The current measurements can also be made by a drifter. In this situation, the exact location of the current measurement can not be predetermined after release. Also drifting measurements can be impacted by other forces such as the wind and waves. This gives a measurement of a current at a specific location and time. The high frequency radar measurements are averaged over a period of time. The depth at which the high frequency radar makes the current measurement is also frequency dependent, but often the upper 1 m is under investigation [*Harlan*, 2003]. This also contributes to the difference between high frequency radar measurements and current meters.

When ship drift is used to measure the current, the surface area of the ship under water

experiencing the ocean current vs. the structure that is above the waterline experiencing the wind effects is a topic of much debate. Aside from different regions having different impacts, i.e. high current-small wind vs. small current-high wind, the ship specific properties including the dimensions of the ship may also have to be taken into consideration. *McPhaden et al.* [1991] and *Arnault* [1987] performed different comparisons between ship drift and other ocean current measurement techniques and were able to determine the annual cycle of the currents from the ship drifts.

2.3 Ocean Currents in San Francisco Bay

As one case study occurs in San Francisco, a brief discussion of the local oceanography is appropriate. San Francisco Bay is comprised of the Suisun, San Pablo, Central and South Bays [*Conomos et al.*, 1985]. The orientation of these bays with respect to each other is depicted in figure 2.1. The Northern Reach is comprised of Suisan Bay, San Pablo Bay and the northern part of Central Bay. This Northern region experiences a non-tidal mean flow that is dependent upon the density, wind and river inflow components [*Peterson et al.*, 1975].

The Southern reach is comprised of South Bay and a portion of Central Bay. South Bay has ocean surface currents that are mixed semi-diurnal in nature from a combination of solar and lunar effects. The magnitude of the major components of the tide for San Francisco are identified in Table 2.1 [*Cheng and Gartner*, 1985]. These first six harmonics of the tides contribute about 85% of the total tidal effects in San Francisco Bay.

Table 2.1: Major Components of the Tide for San Francisco, CA

Tide	*Name*	*Magnitude(cm)*
M2	Principal lunar	57.41
K1	Luni-solar diurnal	36.77
O1	Principal lunar diurnal	22.73
S2	Principal solar	13.57
N2	Larger lunar elliptic	23.14
P1	Principal solar diurnal	11.34

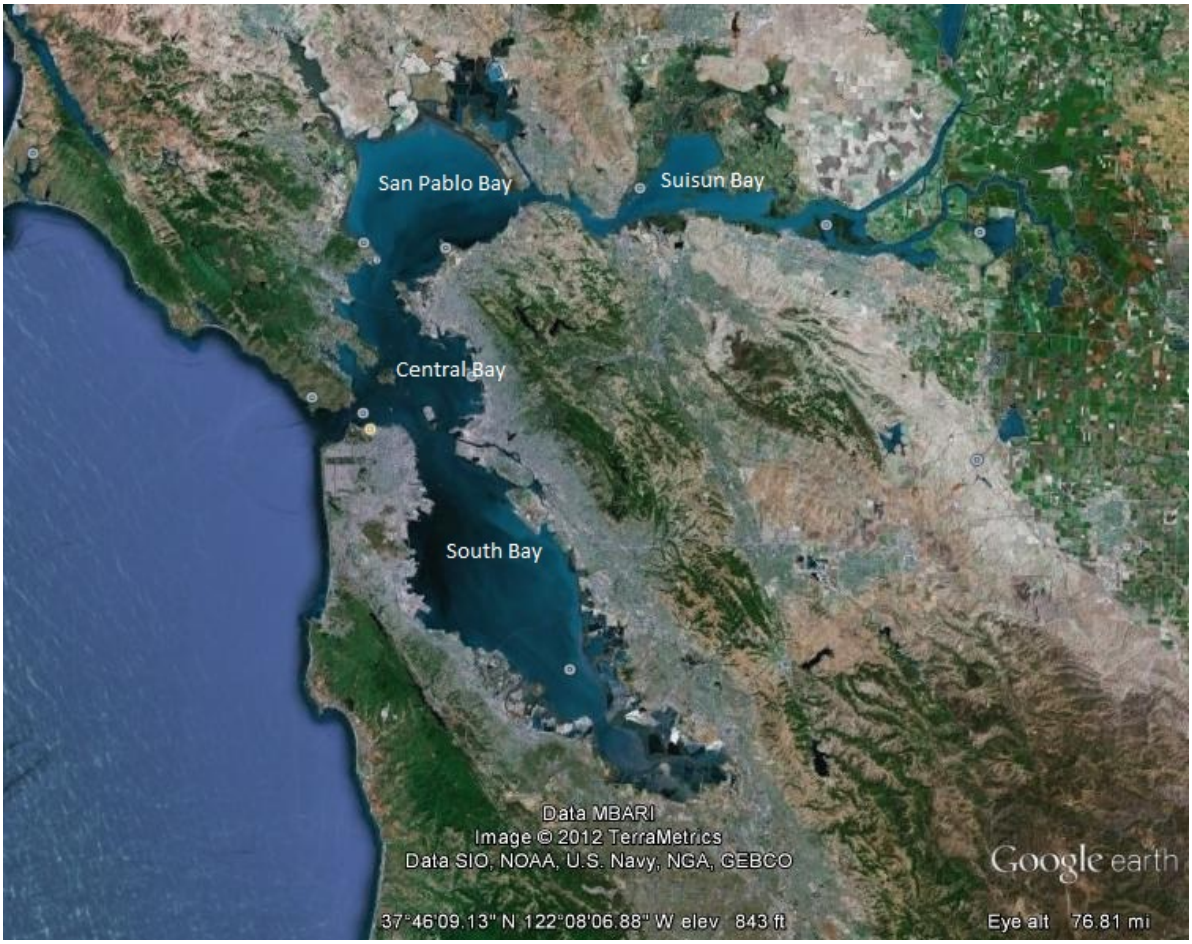

Figure 2.1: Bays that Comprise San Francisco Bay

When the tides are rising, a flood current ensues. When the tides are receding, an ebb current occurs. The National Ocean Service (NOS) estimates the maximum flood and ebb currents for the region at approximately 4 knots [*NOAA*, 2013]. This maximum value is for a location just east of the Golden Gate Bridge.

For this study, total ocean vectors are used and are from a combination of four high frequency radar sites. These sites include the Romberg Tiburon Center, Treasure Island, Crissy Field and Sausalito-Marin City Sanitary District. These locations are depicted in Figure 2.2.

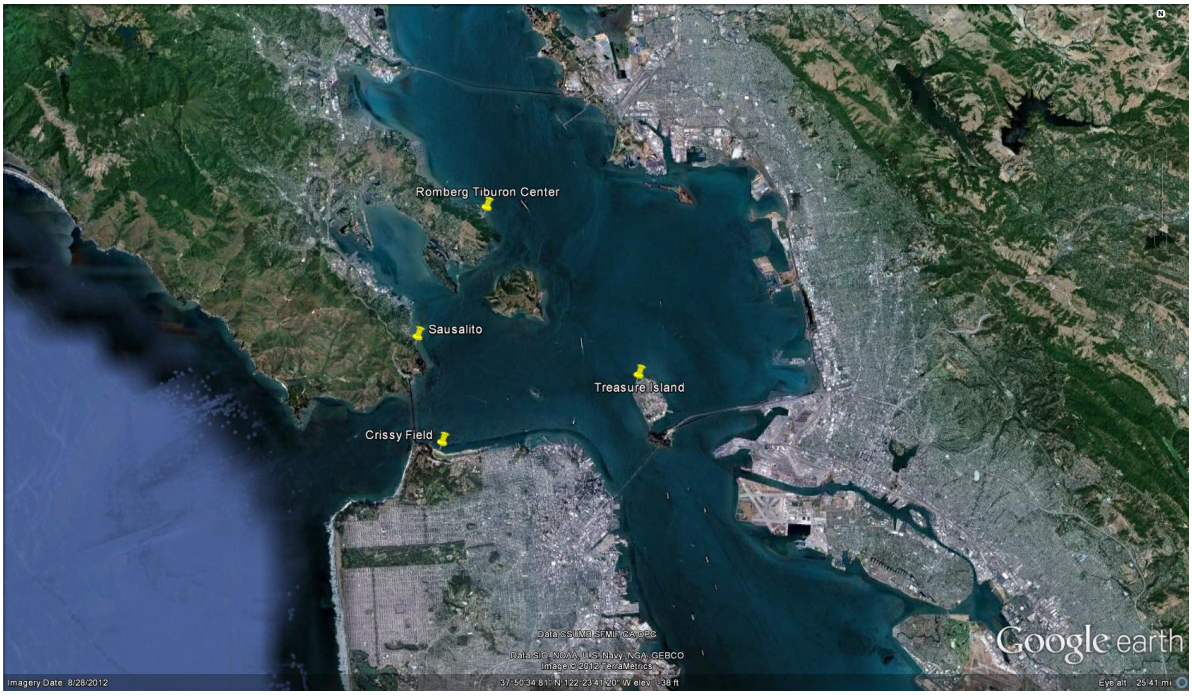

Figure 2.2: High Frequency Radar Sites in San Francisco

2.4 Understanding the Automatic Identification System (AIS)

2.4.1 General AIS Discussion

The AIS is an international standard that facilitates the efficient exchange of information among ships and the shore. AIS functions by collecting and formatting measurements from a ship's sensors into compact messages that are transmitted to nearby ships. This information exchange allows ships to understand the rate and direction of travel of the other ships nearby. This increased awareness helps to reduce the number of accidents at sea. The US Coast Guard uses AIS to increase its knowledge of ship traffic near the US coastline. Additionally, the Coast Guard is investigating ways of obtaining AIS messages from ships farther out from shore than the approximately 25 nautical mile range that the system was originally intended to operate [*Tetreault*, 2002].

The AIS system operates on a Self-Organizing Time Division Multiple Access (SOTDMA) system. Within the SOTDMA system each message is assigned a specific window defined by time. When a message is transmitted, it reserves the next message slot it intends to use so other systems

will not use that slot and consequently reduce any potential conflict for transmission time. Each slot is defined as 26.7 ms in length which allows for 2250 messages every 60 seconds. As AIS operates on two frequencies, 161.975 MHz and 162.025 MHz, there can be a total of 4500 messages each minute [*ITU-R*, 2010]. A specific channel is proposed for long range AIS activities at 156.775 MHz [*Eriksen et al.*, 2010].

The AIS system includes 27 different message types. Table 2.2 lists the subset of message types that are most relevant for this project. The most important message types are the position reports (types 1-3). The position reports contain information such as the ship′s latitude, longitude, heading, course over ground, rate of turn, UTC time of report and navigational status, such as anchored or underway using engine power. In regions with heavy ship traffic, preference is given to position reports over other types of messages because they contain the information necessary for preventing collisions. The UTC date and time are reported in message type 4 to allow different receivers to synchronize their clocks. Message type 5 contains voyage related information related to the ship, like the type of global navigation satellite system (GNSS) in use, the estimated time of arrival, and, the maximum static draught. This message would be of particular interest if investigating the impacts of wind on ship drift measurements. Message type 17 is the GNSS broadcast that contains information such as the differential correction coefficients. This allows the accuracy of the AIS measurements for ship position to improve to better than 10 m. Message type 21 is the Aid to Navigation message. This message, broadcasted from a bouy or fixed device, contains the location of the aid, and is used by receiving vessels as a collision avoidance mechanism. *Chang and Xinyu* [2010] provides an example where this message can be used to determine if an Aid to Navigation has violated the range of its expected location. Last would be message type 27, the Long Range AIS Broadcast message. While this message was specifically designed to be picked up by satellites, it does not include the heading information of the transmitting ship. Therefore, due to the lack of heading information, this particular message does not support ship drift calculations

The specific frequency used to report the various messages depends on the message type and the dynamics of the ship. Position reports will vary in time from once every 2 seconds, for ships

Table 2.2: Subset of AIS Message Types from ITU-R M.1371-4

MessageID	*Name*	Description
1	Position Report	Scheduled position report
2	Position Report	Assigned scheduled position report
3	Position Report	Special position report, response to interrogation
4	Base Station Report	Position, UTC, date and current slot number of base station
5	Static and Voyage Related Data	Scheduled static and voyage related vessel data report
10	UTC/Date Inquiry	Request UTC and date
11	UTC/Date Response	Current UTC and date if available
17	DGNSS Broadcast Binary Message	DGNSS corrections provided by a base station
21	Aids-to-Navigation Report	Position and status report for aids-to-navigation
27	Long Range AIS Broadcast Message	A subset of position report data

traveling above 23 knots, to once every 3 minutes, for ships that are moored.

AIS messages are encoded in a 6 bit binary format that is parsed to describe the message contents. International Telecommunications Union - Recommendation (ITU-R) M.1371-4 describes how to parse the messages. The parsing process can be demonstrated with an example.

An example of the raw data without the receiver header information of a position report from an AIS receiver is below,

13?uwn002EG?;¡jE‘Bu2JipH0¡0?

This 28 character listing is converted into a 168 binary bit sequence. These 168 bits are then parsed using the ITU-R M1371-4 algorithm. The position report produces the following information:

Maritime Mobile Service Identity (MMSI): 218071000

Speed over Ground: 14.9 kts

Position Accuracy: 0 ($\leq$ 10 m)

Longitude: 122.514016 deg W

Latitude: 37.800513 deg N

Course over Ground: 61.9 deg

True heading: 60 deg

Timestamp: 12 secs past the minute

This information indicates the ship is arriving in San Francisco bay. This position report can be combined with a base station report (Message 4), to determine the actual time of the position report. For this dissertation, AIS data was provided by two AIS receivers operated by CloudView Photography [*Cloudview*, 2009]. The AIS receivers averaged 500,000 messages each day for San Francisco Bay with the majority of them being position reports.

2.4.2 Space Based AIS

Several organizations have been investigating the ability to collect AIS messages from space. *Eriksen et al.* [2010] discusses two such initiatives, a nanosatellite from Norway and an ESA funded experiment on the International Space Station (ISS). The Norwegian polar satellite, AISSat-1 detected 500,000 messages from 20 000 unique ships each day. The ESA funded NORAIS receivers on the ISS averaged 350,000 position reports per day and 22,000 unique MMSIs [*Eriksen et al.*, 2010].

ORBCOMM is another satellite constellation that allows for global AIS messages to be transmitted to a common location for processing. Figure 2.3 is an image of 1 million AIS reports that have been detected by ORBCOMM. The shipping lanes are clearly visible in this image and would be optimal locations for ship drift computations from AIS data partially due to the magnitude of data that could be used to help further average an answer. It can also be readily seen that the Northern Hemisphere has more ship traffic than the Southern Hemisphere and so it is assumed

better results could be achieved in the Northern Hemisphere.

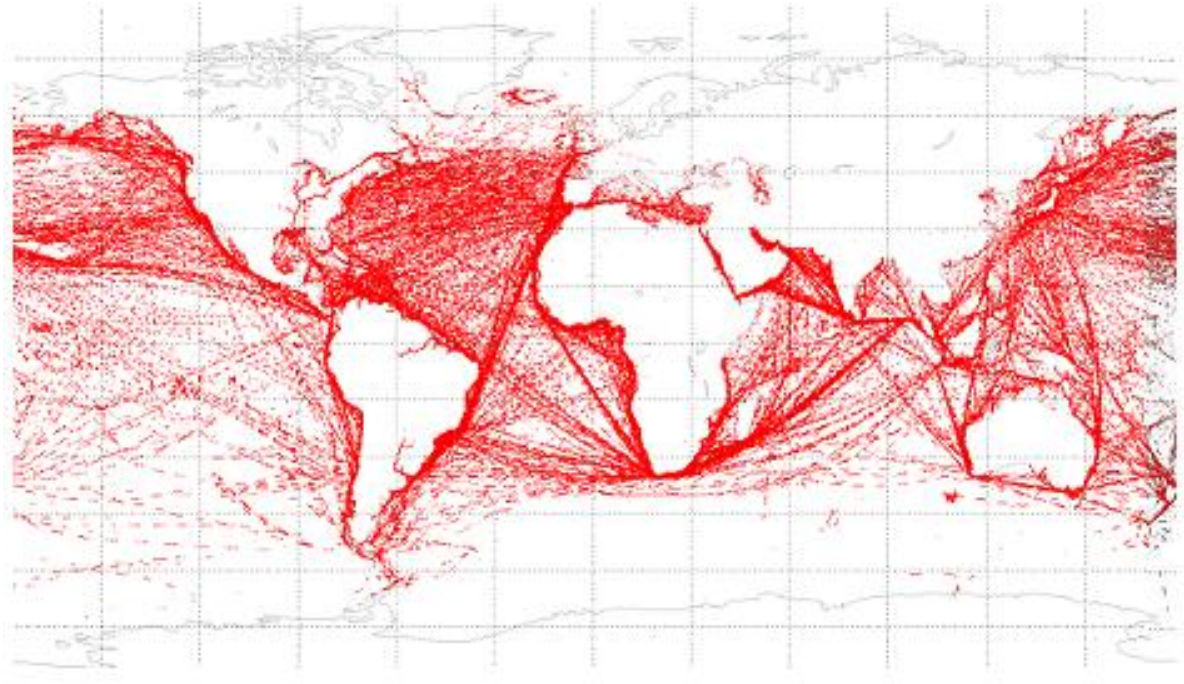

Figure 2.3: 1 Million AIS Messages from [*ORBCOMM*, 2012]

Satellite based AIS helps mitigate some of the issues inherent when working with ship drift data, such as receiving the data in a consistently, globally, and timely manner. Also by having such a large dataset, the ability to detect individual ship′s biases should be improved.

The next chapter discusses how AIS can be applied to the ship drift technique to measure ocean currents.

Chapter 3

AIS Ocean Current Technique

3.1 Using AIS Information to Calculate Ship Drift

The raw AIS measurements contain all of the necessary measurements required to compute a ship drift. A ship drift calculation can be computed with two different position reports. Figure 3.1 presents the ship drift triangle described by *Richardson* [1997] that is used for the computation of the ocean current.

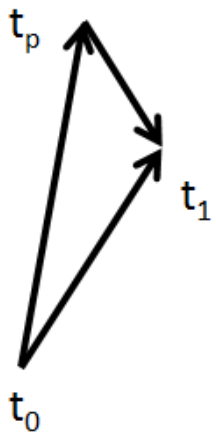

Figure 3.1: Ship Drift Triangle

From Figure 3.1, the ship location at the time of the initial ship report is designated as t_0. The actual ship location at the time of the second AIS measurement is at point t_1. T_p is the location of the ship had it continued on it's heading direction. Therefore, the actual distance vector is between points t_0 and t_1. The dead reckoning vector is the vector between t_0 and t_p. The vector

that is the difference between these two is the amount of ship displacement.

3.2 Actual Distance Traveled

The actual distance traveled can be computed from two different AIS messages. Each position report contains the latitude and longitude of either the starting location at t_0 or the final location when at t_1. While a simple differencing of the latitude and longitude points between the messages could be used, equations 3.1 - 3.3, depict the use of the haversine formula instead. These equations are better conditioned when there are small distances involved [*Sinnott*, 1984]. Equation 3.1 is the square of half the chord length between the AIS position reports. The angular distance between these points is computed from equation 3.2. Last, this angle is scaled by the radius of the Earth, R, in equation 3.3 to compute the actual distance traveled D_{act}.

$$a = \sin^2((latdiff)/2.0) + \cos(lat1) * \cos(lat2) * \sin^2((londiff)/2.0) \tag{3.1}$$

$$c = 2.0 * atan2(\sqrt{a}, \sqrt{1-a}) \tag{3.2}$$

$$D_{act} = R * c \tag{3.3}$$

3.3 Dead Reckoning Vector

The dead reckoning vector is computed from the initial AIS position report for speed over ground and the difference in time stamps between the two reports. By multiplying the speed over ground (sog) by the time difference between the position reports, the length of the dead reckoning vector can be computed. This vector is in the direction of the true heading and as such provides an orientation of this vector with respect to the compass. The equation to compute this dead reckoning vector, D_{dr} is shown in equation 3.4.

$$D_{dr} = sog * (t_1 - t_0) \tag{3.4}$$

3.4 Ship Displacement

The ship displacement can be solved for by computing the difference between the actual distance traveled vector and the dead reckoning vector. To accomplish this, the actual distance vector is decomposed into x and y components as well as components for the dead reckoning vector. When the actual distance travel vector is subtracted from the dead reckoning vector, the amount the ship has been displaced can be computed.

$$D_{sd_x} = D_{dr} * \cos(head) - D_{act} * \cos(cog) \tag{3.5}$$

$$D_{sd_y} = D_{dr} * \sin(head) - D_{act} * \sin(cog) \tag{3.6}$$

The magnitude of the ship displacement can be computed by equation 3.7

$$D_{sd} = \sqrt{D_{sd_x}^2 + D_{sd_y}^2} \tag{3.7}$$

Once this distance is computed, simply dividing by the time between measurements gives the magnitude of the ocean surface current magnitude, OC_{ship}, equation 3.8.

$$OC_{ship} = \frac{D_{sd}}{(t_1 - t_0)} \tag{3.8}$$

3.5 Ocean Current Direction

With the ship displacement broken up into components, the ocean current direction can be solved for with the atan2 function. This arctangent function with quadrant checks applies to all different configurations, and readily solves for the direction of the ocean current.

To ensure that each quadrant was computed correctly a relationship table between the true heading and the course over ground for vectors of the same length for certain key angles is presented in table 3.1.

Table 3.1: Ocean Current Direction of COG vs True Heading

		Course over Ground							
		30	60	120	150	210	240	300	330
Heading	30	X	135	165	180	X	225	255	270
	60	315	X	180	195	225	X	270	285
	120	345	0	X	225	255	270	X	315
	150	0	15	45	X	270	285	315	X
	210	X	45	75	90	X	315	345	0
	240	45	X	90	105	135	X	0	15
	300	75	90	X	135	165	180	X	45
	330	90	105	135	X	180	195	225	X

As an example, for a ship to have a true heading of 30° but have a course over ground of 150°, the ocean current must be traveling in the 180° direction. The table illustrates some angle combinations that provide ocean current directions in the North, South, East and West orientations.

Also the table illustrates for certain angles the ocean current direction cannot be computed with this method alone. This occurs when the dead reckoning vector and the actual distance travel vector are in the same line. In this special case, the current direction is either in the direction of ship travel or 180° in the opposite direction, or there is possibly no current at all. The magnitude and orientation can be computed by the difference in predicted dead reckoning position and the actual position. If these two vectors are of the same length, there is no current. If the dead reckoning vector is longer, the ship is heading directly into the current. Last if the actual distance traveled is longer, the ocean current is coming from behind the ship and pushing it along further.

Another assumption that should be explicitly called out is the above procedure works in situations where the ship is running straight. More advanced techniques could be used to solve for the ocean current of a turning ship but is beyond the scope of this dissertation.

Another method of computing the ocean current would be to divide the actual distance

traveled by time and perform the law of cosines computation on vectors in the units of m/s. This approach was not selected for this dissertation as by computing the distances and then normalizing by time, it may be easier to see where the individual error sources are originating. A description of those errors and how they propagate through the computations is provided in the next chapter.

3.6 Other AIS Items to Consider For Future Research

The procedure stated above only uses messages 1-4 to compute a ship drift. The static ship and voyage related data, message 5, includes information about the length of the ship and well as the ship's draught [*ITU-R*, 2010]. This information may be useful in helping to further quantify the windage effect on a particular ship. This investigation is beyond the scope of this dissertation.

Chapter 4

Error Propagation

4.1 Propagation of AIS Measurement Uncertainties

Computing ocean currents from AIS based ship drift computations comes with several error sources. The ship drift technique itself is subject to error as additional external forces impact the ship other than ocean currents. These forces include such effects as wind and wave forces. Richardson (1997) has performed some work quantifying the wind effect on ship drift computations and is beyond the scope of this dissertation. Other error sources that would apply to AIS based ship drift measurements include ship specific biases and message uncertainty. As ship specific biases can not be addressed systematically, the focus of the error propagation has been on the precision of the AIS messages and how that measurement uncertainty combines throughout the ocean current computation process.

Taylor [1997] provides a discussion for the propagation of these uncertainties. The propagation equations used in this dissertation, equation 4.1 - equation 4.6, are repeated from *Taylor* [1997] below for convenience. q is the quantity in question and x, z, u and w are the variables that contribute to q. The 6 types of propagation of uncertainty equations include:

1) sum and difference: $q = x + ... + z - (u + ... + w)$

$$\delta q = \sqrt{(\delta x)^2 + ... + (\delta z)^2 + (\delta u)^2 + ... + (\delta w)^2} \tag{4.1}$$

2) product and quotient: $q = \frac{x \times ... \times z}{u \times ... \times w}$

$$\frac{\delta q}{|q|} = \sqrt{\left(\frac{\delta x}{x}\right)^2 + ... + \left(\frac{\delta z}{z}\right)^2 + \left(\frac{\delta u}{u}\right)^2 + ... + \left(\frac{\delta w}{w}\right)^2} \tag{4.2}$$

3) multiplication by a scalar factor: $q = Bx$

$$\delta q = |B|\delta x \tag{4.3}$$

4) an equation that is a function of one variable: $q(x)$

$$\delta q = \left|\frac{dq}{dx}\right| \delta x \tag{4.4}$$

5) a function that involves a power: $q = x^n$

$$\frac{\delta q}{|q|} = |n|\frac{\delta x}{|x|} \tag{4.5}$$

6) a function of several variables: $q(x, ..., z)$

$$\delta q = \sqrt{\left(\frac{\delta q}{\delta x}\delta x\right)^2 + ... + \left(\frac{\delta q}{\delta z}\delta z\right)^2} \tag{4.6}$$

In the later description of the error propagations these equations will be referenced to help delineate the steps that are being taken.

4.2 AIS Measurement Precision

The same equations that were described in chapter 3, will be discussed here with the associated uncertainty, and a description of how that uncertainty changes with each computation.

In order to compute a ship drift from AIS measurements, a total of 6 different measurement types are needed. The precision of these measurement types are identified in Table 4.1.

Converting some of the measurement types to metric units for ocean current computations results in some scaling to the uncertainty. The speed over ground in knots is converted to meters per second. This conversion is shown in equation 4.7.

Table 4.1: Precision of AIS Measurements

Measurement type	Precision	units
Latitude	1/10000	min
Longitude	1/10000	min
Time	1.0	s
Speed over Ground	0.1	kts
Course over Ground	0.1	Deg
Heading	1.0	Deg

$$sog_{m_s} = sog_{kts} * 1852.0/3600.0 \tag{4.7}$$

This simply scales the uncertainty of the speed over ground measurement by the same amount. Equation 4.8 shows the steps from taking the 0.1 kts uncertainty and scaling it accordingly to a 0.51 m/s uncertainty using the multiplication by a scale factor, equation 4.3.

$$\sigma sog_{m/s} = \sigma sog_{kts} * 1852.0/3600.0 \tag{4.8}$$

Similar scaling of the uncertainty measurements are performed for the other measurement types. These scalings include converting the heading, course over ground, latitude and longitude to radians. The updated uncertainty scaling is displayed in Table 4.2.

Table 4.2: Precision of AIS Measurements after Metric Conversions

Measurement type	Precision	units
Latitude	2.9e-8	rad
Longitude	2.9e-8	rad
Time	1.0	s
Speed over Ground	0.051	m/s
Course over Ground	1.7e-3	rad
Heading	1.7e-2	rad

Another assumption related to the reporting accuracy of the AIS measurement is, the measurand should be rounded to the closest reported value. As such, each of these measurand uncertainties

could be reduced by half. An example of this is since time is reported to the nearest second, the actual time and the reported time of the measurement will be different by less than 0.5 seconds.

4.3 Ship Drift Intermediate Product Error Computations

To compute the effects that the errors have on the uncertainty of the ocean current measurement, the errors at intermediate steps are computed. These errors include the uncertainty of the computed course deviation of the ship due to all the external forces. The intermediate products that are computed as part of the ship drift computations are listed in table 4.3.

Table 4.3: Intermediate Errors for Ship Drift Computations

Intermediate Products	Symbol	AIS Measurands
Actual Distance	D_{act}	m
Dead Recoking	D_{dr}	m
Angular Uncertainty between the Vectors	η	rad
Computed Ship Displacement	D_{sd}	m

When computing the propagation errors, they are computed in several steps. Errors from the actual distance traveled, the predicted distance traveled, and how these errors combined with angle uncertainties contribute to the computed ocean distance all need to be understood. These errors can then be used for the ocean current magnitude and the ocean current direction errors.

4.4 Actual Distance Errors

To compute the distance between the two AIS measurements, the Haversine formula is used as it is better conditioned for short distances [*Sinnott*, 1984]. The difference in latitude between the AIS measurements needs to be computed. The propagation of uncertainty associated with finding the difference of two latitudes is described by equation 4.9, the propagation equation for the sum or difference of two variables.

$$\sigma_{latdiff} = \sqrt{\sigma_{lat1}^2 + \sigma_{lat2}^2} \tag{4.9}$$

This same equation is repeated for the difference in longitude and the difference in time between the two AIS measurements. The next series of equations are used to determine the actual distance the ship traveled between the two AIS measurements. The first intermediate equation of the haversine formula is equation 4.10, the square of half the chord length between the points.

$$a = \sin^2((latdiff)/2.0) + \cos(lat1) * \cos(lat2) * \sin^2((londiff)/2.0) \tag{4.10}$$

By substitution, 4.10 can be rewritten as

$$a = \overbrace{\sin^2\left(\frac{latdiff}{2.0}\right)}^{m1} + \overbrace{\cos(lat1) * \cos(lat2) * \sin^2\left(\frac{londiff}{2.0}\right)}^{m2} \tag{4.11}$$

The uncertainty of the m1 term can be expressed as 4.14 using the propagation of uncertainty for functions with exponents,

$$\sigma q = |q||n|\frac{\sigma x}{x} \tag{4.12}$$

where

$$\begin{aligned} x &= \sin\tfrac{latdiff}{2.0} \\ n &= 2.0 \\ \sigma x &= \sigma latdiff \tfrac{\cos\frac{latdiff}{2.0}}{2.0} \\ q &= m1 \end{aligned}$$

The σx equation was solved for by the uncertainties associated with the function of one variable

$$\sigma x = |\frac{dx}{dl}|\sigma l \tag{4.13}$$

$$\sigma_{m1} = \frac{\sigma_{latdiff}\frac{\cos(\frac{latdiff}{2.0})}{2.0}}{\sin(\frac{latdiff}{2.0})} 2.0 \sin^2(\frac{latdiff}{2.0}) \tag{4.14}$$

The uncertainty associated with m2 can similarly be solved by using a series of substitutions.

$$m2 = \overbrace{\cos(lat1)}^{m2_1}\overbrace{\cos(lat2)}^{m2_2}\overbrace{\sin^2\frac{londiff}{2.0}}^{m2_3} \tag{4.15}$$

where the uncertainty of each of these parts is computed by the uncertainty of a function of one variable equation.

$$\begin{aligned}
\sigma_{m2_1} &= \sigma_{lat1}\sin(lat1) \\
\sigma_{m2_2} &= \sigma_{lat2}\sin(lat2) \\
\sigma_{m2_3} &= \frac{\sigma_{londiff}\frac{\cos\left(\frac{londiff}{2.0}\right)}{2.0}}{\sin\left(\frac{londiff}{2.0}\right)}2.0\sin^2\left(\frac{londiff}{2.0}\right)
\end{aligned}$$

Once these uncertainties are computed individually, they can be combined by the product rule for uncertainties.

$$\sigma q = |q|\sqrt{\left(\frac{\sigma_{m2_1}}{m2_1}\right)^2 + \left(\frac{\sigma_{m2_2}}{m2_2}\right)^2 + \left(\frac{\sigma_{m2_3}}{m2_3}\right)^2} \tag{4.16}$$

The uncertainty of a, the square of half the chord length, can then be computed from the addition rule for uncertainties, equation 4.17

$$\sigma_a = \sqrt{(\sigma m1)^2 + (\sigma m2)^2} \tag{4.17}$$

Now that the uncertainty of a has been computed, the uncertainty of the angular distance in radians can be computed. The angular distance is denoted by equation 4.18.

$$c = 2.0 * atan2(\sqrt{a}, \sqrt{1-a}) \tag{4.18}$$

The quotient rule for uncertainty is used and the uncertainty of the angular distance is described by equation 4.19

$$\sigma c = \frac{\sqrt{a}}{\sqrt{1-a}}\sqrt{\left(\frac{\sigma\sqrt{a}}{\sqrt{a}}\right)^2 + \left(\frac{\sigma\sqrt{1-a}}{1-a}\right)^2} \tag{4.19}$$

Scaling the angular distance in radians by the radius of the Earth allows for the actual distance between the two AIS measurements to be known in meters.

$$D_{act} = R * c \tag{4.20}$$

The uncertainty associated with the actual distance can be computed simply by scaling the uncertainty of the angular distance in radians by the radius of the Earth.

4.5 Dead Reckoning Errors

The predicted distance is computed by

$$D_{dr} = sog_{m/s} * (t_1 - t_0) \tag{4.21}$$

As both the sog and the difference in time were discussed previously, the combination of these error terms is accomplished via the product rule for uncertainty propagation, equation 4.22

$$\delta_{dr} = D_{dr}\sqrt{(\delta_{sog}/sog)^2 + (\delta_{time}/(t_1 - t_0))^2} \tag{4.22}$$

4.6 Ocean Current Magnitude Errors

This ship displacement is computed by calculating the components of the actual distance traveled and the dead reckoning vector. The errors associated with actual distance traveled are described by equations 4.23 and 4.24. The corresponding errors associated with breaking the dead reckoning vector into components is described by equations 4.25 and 4.26.

$$\delta_{act_x} = \sqrt{(\cos{(cog)} * \delta_{act})^2 + (D_{act} * -1 * sin(cog) * \delta_{cog})^2} \tag{4.23}$$

$$\delta_{act_y} = \sqrt{(\sin{(cog)} * \delta_{act})^2 + (D_{act} * cos(cog) * \delta_{cog})^2} \tag{4.24}$$

$$\delta_{dr_x} = \sqrt{(\cos{(heading)} * \delta_{dr})^2 + (D_{dr} * -1 * sin(heading) * \delta_{heading})^2} \tag{4.25}$$

$$\delta_{dr_y} = \sqrt{(\sin{(heading)} * \delta_{dr})^2 + (D_{dr} * cos(heading) * \delta_{heading})^2} \tag{4.26}$$

With an understanding of the component errors, these terms can be combined to describe the difference in vectors.

$$\delta_{sd_x} = \sqrt{\delta_{act_x}^2 + \delta_{dr_x}^2} \tag{4.27}$$

$$\delta_{sd_y} = \sqrt{\delta_{act_y}^2 + \delta_{dr_y}^2} \tag{4.28}$$

These errors can be combined to solve for the errors associated with ship displacement according to 4.29.

$$\delta_{sd} = D_{sd} * \frac{1}{2} * \frac{\sqrt{(2 * D_{sd_x} * \delta_{dx})^2 + (2 * D_{sd_y} * \delta_{dy})^2}}{(D_{sd_x}^2 + D_{sd_y}^2)} \tag{4.29}$$

The ship displacement when divided by the difference in time in the AIS measurements, results in the ocean current magnitude error. This error can be computed according to equation 4.30.

$$\delta_{oc} = \frac{D_{sd}}{t_2 - t_1} * \sqrt{\left(\frac{\delta_{sd}}{D_{sd}}\right)^2 + \left(\frac{\delta_{time}}{t_1 - t_0}\right)} \tag{4.30}$$

4.7 Ocean Current Direction Error

The ocean current direction error can be solved for based on the equation for errors in an equation with multiple variables for the atan2 function, equation 4.31. A 180 degree rotation of the values may be necessary based on the derivative, but the errors would be independent of that fact.

$$\delta_{ocdir} = \sqrt{\left(\frac{-D_{sd_y}}{D_{sd_x}^2 + D_{sd_y}^2} * \delta_{sd_x}\right)^2 + \left(\frac{D_{sd_x}}{D_{sd_x}^2 + D_{sd_y}^2} * \delta_{sd_x}\right)^2} \tag{4.31}$$

With an understanding of how the errors with this process are computed, understanding the sensitivity of this analysis is an important aspect to understand next.

Chapter 5

AIS Ocean Current Sensitivity

The manner in which the AIS measurements are combined involves a trade off between the resolution of the current that can be measured and the errors of the measurement. If short time measurements are selected, small current features can be measured. If a longer integration time is selected, larger scale currents can be measured. With each of these decisions, implications to the error terms result. This chapter seeks to identify common trends that can be used to assist with determining if an ocean current measurement from AIS can be trusted.

5.1 Comparison of AIS Based Ship Drift to Literature

Richardson and McKee [1984] estimated the errors associated with the ship drift computation they were performing at approximately 20 cm/s. They were able to average this down to around 2 cm/s based on the number of ships they had in the grid for each month. These errors assumed a $\pm$ 2 km error in position, a $\pm$ 1° error in heading and a $\pm$ 0.3 kts error in speed over ground.

The AIS messages have reporting limits that are smaller than the limits used by *Richardson and McKee* [1984]. With the rise of Global Navigation Satellite Systems (GNSS) with systems such as GPS, the position of a ship can be determined more accurately than in the 1980s. The AIS message provides a mechanism whereby if the differential GPS corrections are used, position uncertainties can be less than 10 m. Similarly, the speed over ground can be reported to the closest 0.1 kts, or an accuracy of $\pm$ 0.05 kts. The heading also has a minor improvement. Headings can be reported to the closest degree, or to an uncertainty of $\pm 0.5°$. With these new tolerances used for

a ship traveling for a 12 hour period at a nominal speed of 10 kts, the precision with which a ship drift measurement can be made improves from approximately 20 cm/s to approximately 3 cm/s, based on AIS message reporting tolerances.

The order of magnitude improvement in ship drift precision could be used differently depending on the goals of the study. The better precision, could help reduce the errors of any large scale analysis that have previously been performed with ship drift. The better precision could also be used to assess smaller scale features while keeping the errors on the same level as historical analyses. The better precision may also assist in improving the studies that investigate effects such as the wind on ship drift.

5.2 Observations about sensitivity of performance

5.2.1 Actual distance and associated error terms

To simplify some of the calculations stated previously, the position measurements may be accurate to within 10 m for high accuracy ships using differential GNSS location systems. If this 10 m uncertainty is applied to both the starting and the finishing locations, a constant error term is computed for the actual distance component of the ship drift computation. As the error is constantly 14.14 m regardless of the amount of distance traveled, longer distances would provide more accurate ocean current measurements as the ratio of the error term over the distance traveled would decrease for longer distances. Figure 5.1 displays a trend for how the percent error of the actual distance decreases with larger distances between AIS measurements.

So for a ship that traveled 100 m, there would be a 14% error in the actual distance traveled. If a larger scale ocean current was measured, such as one with a scale of 1000 m, a 1.4% error would be the result of the computed actual distance traveled. Consequently, a smaller percentage of error will occur for larger distances between AIS measurements.

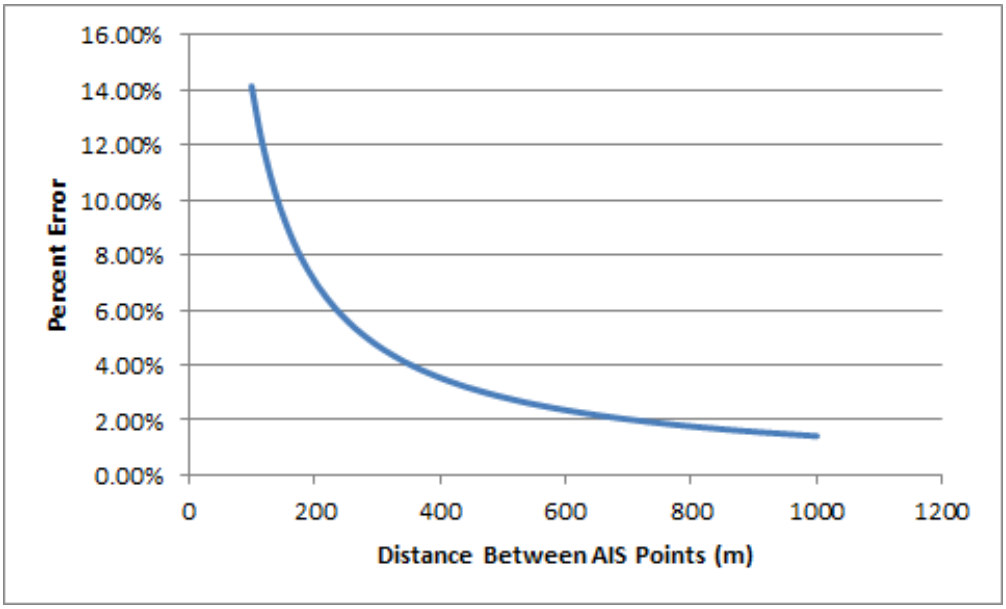

Figure 5.1: Percent Error for Actual Distance based on Distance between AIS points

5.2.2 Consecutive AIS measurements

As the AIS measurements frequency changes with respect to how quickly a ship is moving, consecutive measurements may not be all that different. The ITU recommendation states the frequency for which ships must report their position. A subset of that table appears in table 5.1 along with the distance a ship traveled over that time interval.

Table 5.1: AIS Reporting Frequency Impact on Distance Traveled

Ship's Speed	Nominal reporting interval	Approx. Distance Traveled per Interval (m)
14 kts	10 s	72.0
23 kts	6 s	71.0
$\geq 23kts$	2 s	23.6

A plot of all the ship distances traveled between consecutive measurements is shown in figure 5.2. As the distance does not exceed 72 m, as described in section 5.2.1, the actual distance traveled will have at least a 19% error due to consecutive measurements. This rapid measurement between adjacent ship locations degrades the usefulness of computing ocean currents from

consecutive measurements.

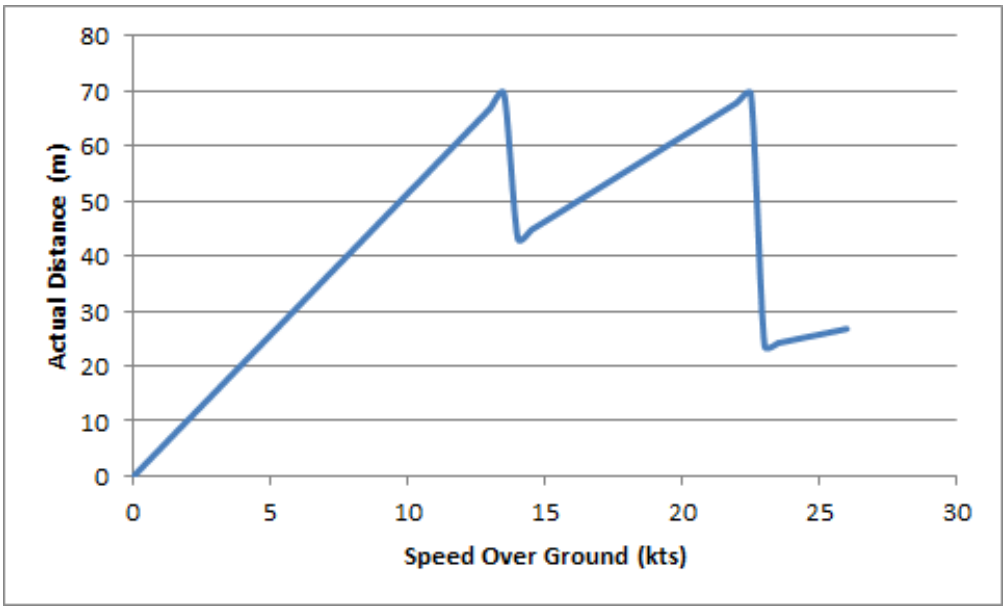

Figure 5.2: Distance Traveled Between AIS Measurements by Ship Speed

5.2.3 Simulated Angle Sensitivity Results

Weak ocean currents and their effect on computed ship drift ocean currents, was pointed out in *DeHaan* [1998]. An extension of this is the orientation the ship makes with respect to the ocean current has a large effect on the signal to noise ratio (SNR), i.e. if a ship is traveling perpendicular to the current, the ship will be displaced a larger distance. Therefore, the larger the difference between the heading and course over the ground, the stronger the SNR and the smaller the error. To illustrate this point, the ocean current error computed for a ship drift of varying angles between the dead reckoning vector and an actual distance vector of the same length is presented in figures 5.3 through 5.8. For this series of graphs, the actual distance vector and the dead reckoning vector were simulated to have the same length. These vectors were varied from a 1° separation to the east, to a 1° separation to the west. This results in some artificially large ocean current computations, but the values are consistent with the simulated input. The simulated ship was also assumed to be traveling at 10.0 kts.

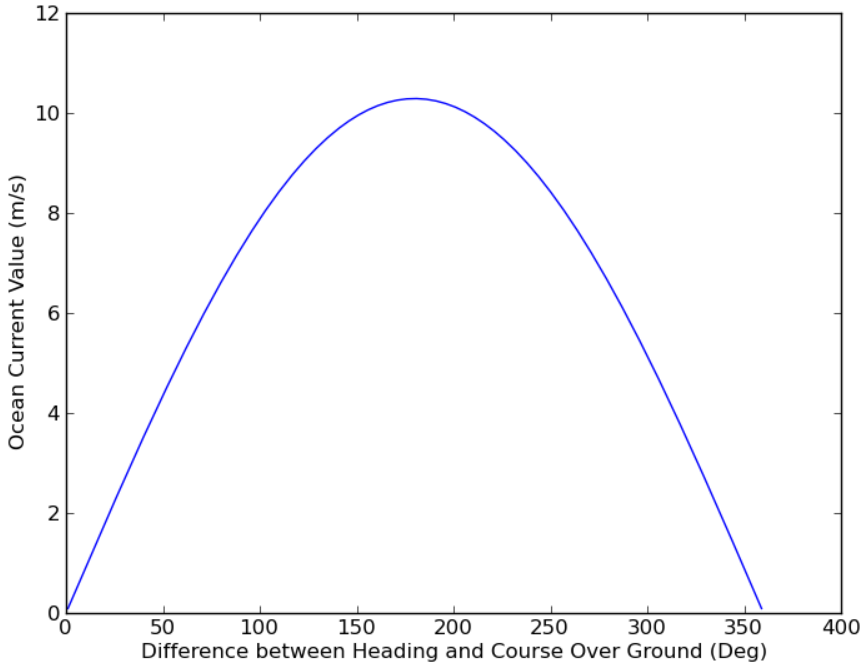

Figure 5.3: Difference between Heading and Course Over Ground vs. Ocean Current Magnitude

Figure 5.3 depicts how the ocean current increases for the larger angles between the heading vector and the dead reckoning vector. With this simulated data, a ship traveling at 10 kts (5.14 m/s), with the 180° separation will result in approximately a 10.28 m/s ocean current to obtain the necessary ship displacement. With smaller angles between the heading and course over ground, a smaller ocean current magnitude is required to achieve this displacement. The error of the ocean current magnitude also increases with a larger angle between the heading and course over ground, figure 5.4.

The error ratio, defined as the ocean current magnitude error over the ocean current magnitude, decreases for the larger angle separation. This error ratio is proportionally quite large for the small angles. This implies either weak surface current measurements or an orientation of the ship is with or against the current. This intuitively makes sense as the closer the vectors are in relation to each other, the more possible combinations of ocean current vectors that can be drawn between them.

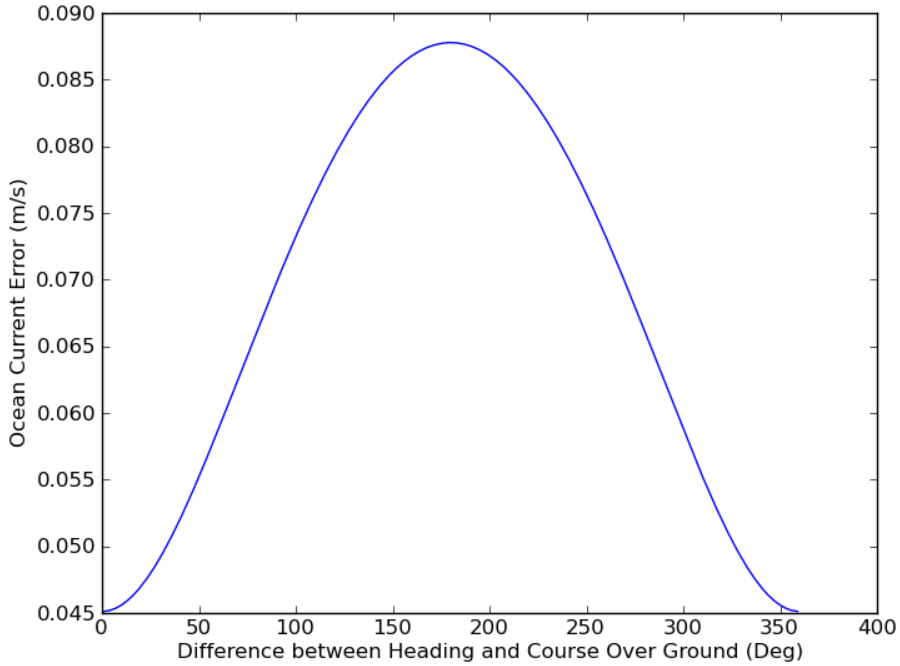

Figure 5.4: Difference between Heading and Course Over Ground vs. Ocean Current Magnitude Error

Figure 5.6 depicts how the ocean current direction changes with respect to the angle between the heading and the course over ground. For a 1° separation between the heading and the course over ground, an ocean current just larger than 90° from the heading must exist to produce this example. If the heading and the course over ground are in opposite directions, the ocean current direction must be in the direction of the course over ground. Therefore figure 5.6 goes from 90° for the ocean current, through 180° and ultimately to just below 270°.

The error associated with the ocean current direction is the greatest when there is a small angle difference between the heading and the course over ground. This larger error is the result of having a larger amount of overlap in the error bounds to the actual distance vector and the dead reckoning vector error bounds. The ocean current error ratio also shows how the errors are larger for the small angles between the heading and the course over ground, figure 5.8.

Ultimately, the trend for both the ocean current magnitude and the ocean current direction

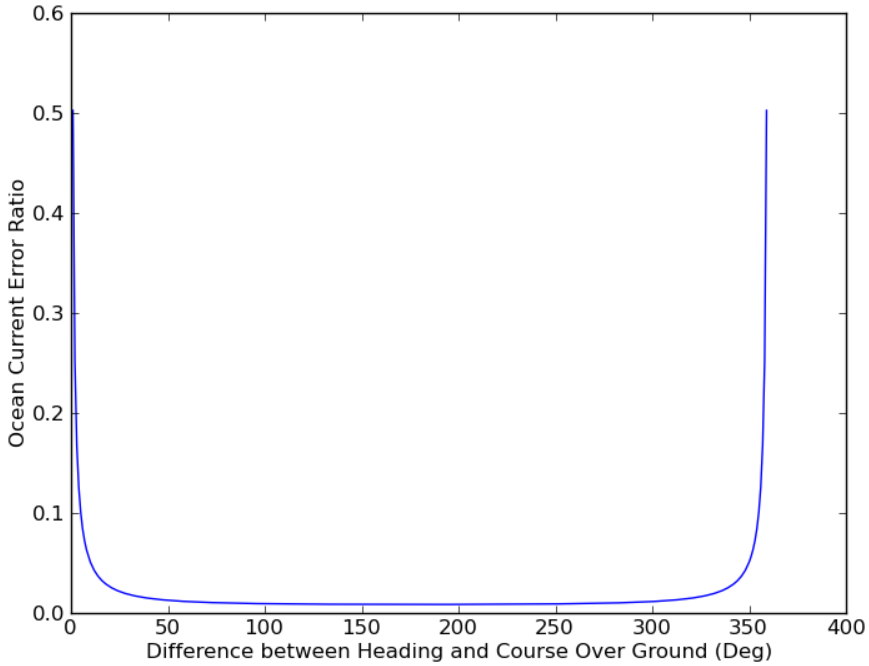

Figure 5.5: Difference between Heading and Course Over Ground vs. Ocean Current Magnitude Error Ratio

will have proportionally less error when the angle difference between the course over ground and the heading is larger.

5.2.4 Sensitivity Based on the Speed of the Ship

Another variable that was investigated to determine a trend on the ocean current measurement is the speed of the ship. Does the frequency of an AIS message support more accurate measurements for slow moving or fast moving ships? The speed of the ship directly impacts the measurement of the dead reckoning distance. The errors in the dead reckoning distance were computed assuming the .1 kts uncertainty in speed over ground and a 0.5 s uncertainty for each AIS measurement in time. Therefore, the product rule for uncertainties was used, equation 5.1 in this example.

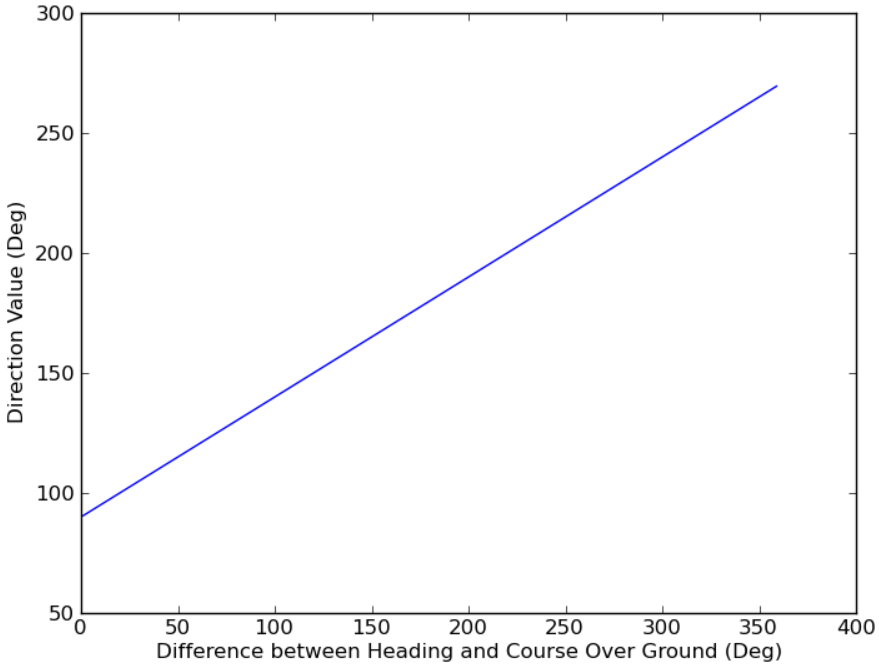

Figure 5.6: Difference between Heading and Course Over Ground vs. Ocean Current Direction

$$\delta dr = \|dr\| \sqrt{\left(\frac{\delta sog}{sog}\right)^2 + \left(\frac{\delta\left(t_1 - t_0\right)}{t_1 - t_0}\right)^2} \tag{5.1}$$

Table 5.2 presents how the speed of a ship over a constant 60 sec time interval impacts the dead reckoning distance error.

Table 5.2: Speed over Ground Dependency on Dead Reckoning Distance

Speed over Ground	5 kts	10 kts	20 kts
Dead Reckoning Distance (m)	154.3	308.7	617.3
Dead Reckoning Error (m)	3.58	4.77	7.90
% Error	2.3	1.5	1.3

Integrating across a constant timeframe, the faster moving ships had a proportionally smaller error than the slower moving ships. This is a similar conclusion to section 5.2.1 where the larger distance traveled ships had a smaller error for the actual distance traveled.

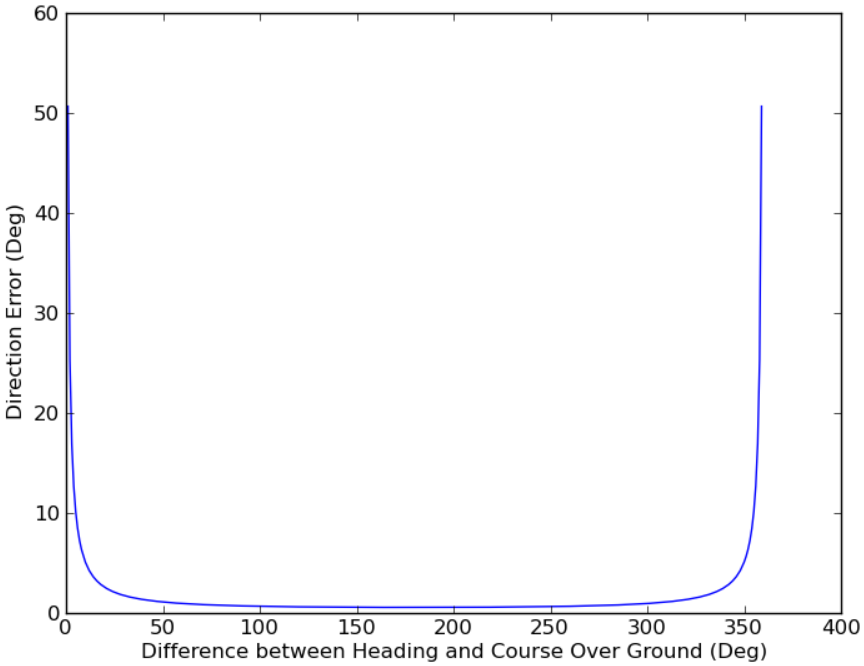

Figure 5.7: Difference between Heading and Course Over Ground vs. Ocean Current Direction Error

5.3 General Sensitivity Trends

Examining the sources of errors for the dead reckoning vector, the actual distance traveled, the angle between them, and ship speed, the ship that would give the smallest overall error would be the one traveling larger distances between measurements, at a faster speed, with a larger angle between the true heading and the course over ground. With this knowledge, the recommendation would be to compute the ocean current measurements based on the time and speed of the ship when considering the scale of the ocean current of interest.

5.4 Other Observations about Ship Drift Sensitivities

The ship drift computation appears to be the most susceptible to the angle between the true heading and the course over ground. Improvements to the ability to measure the true heading would be helpful in reducing the total ocean current error from AIS based ship drifts.

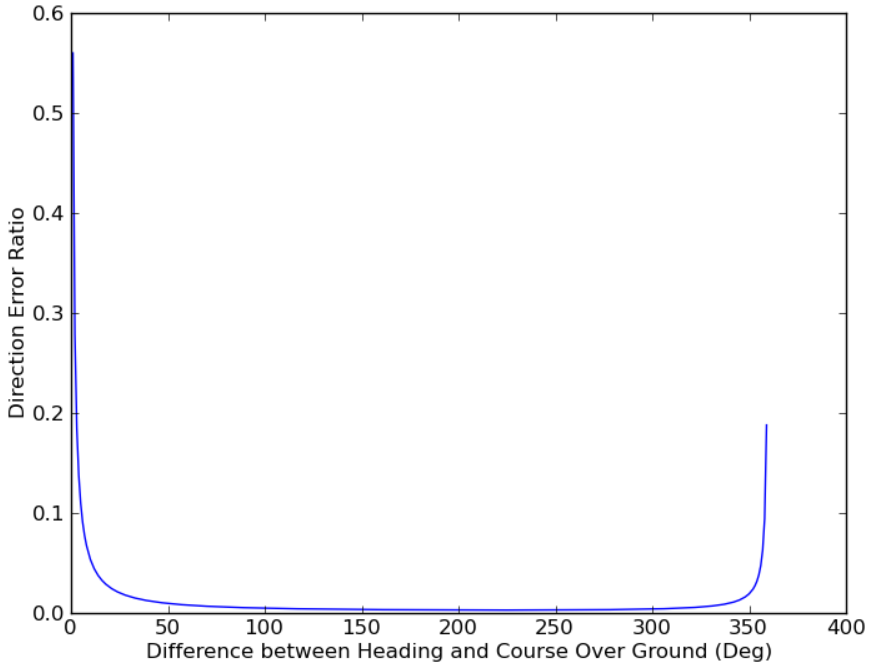

Figure 5.8: Difference between Heading and Course Over Ground vs. Ocean Current Direction Error Ratio

The historical ship drift analysis, with time periods of 12-24 hours, could ignore the transient effects of the ship's speed and it could be assumed the ship was traveling at a constant speed. Working with smaller distances and quicker times, an additional step of ensuring the ship is traveling at a consistent speed or multiple ship drift intervals should be used. Otherwise it is possible to have the ship's increase or decrease in speed corrupt the ocean current estimate.

Chapter 6

Validation of AIS based Ship Drift to other Ocean Current Sources

Some relevent discussions and analyses that involve using AIS messages to assist in determining ocean currents are discussed below:

1) Generic ship drift computations from AIS Measurements.

2) A comparison of ship drift data to high frequency radar measurements in San Francisco Bay.

3) AIS data and ship drift compared to an ocean model in the Gulf of Mexico.

4) A comparison of AIS data to ocean current predictions for moored ships.

Each dataset has its advantages and disadvantages, however common trends between the datasets can be observed. The datasets were provided by a variety of sources. The open ocean AIS data is provided by ORBCOMM. The HYCOM ocean model is produced by a consortium of groups. The AIS data in San Francisco is provided by Cloudview Photography. The high frequency radar data for San Francisco Bay is provided by San Francisco State University.

6.1 Generic Ship Drift Computations from AIS Measurements

While the previous chapter discussed some theoretical aspects of working with AIS messages for ship drift computations, working with real data proves to be a bit more complex. A large amount of AIS data pertains to ships that are not moving but are still required to report this position once every three minutes. This data can not be used for ocean current computations. Also two underlying assumptions about ship drift computations are that ships are traveling in a straight

line and at a constant speed. This further reduces the number of AIS messages that can be used for ocean current computations. Consequently, the filter limits selected for use required the ship to have a heading that varies by less than 2^o.

6.2 AIS Ship Drift and High Frequency Radar Comparison

The next analysis involves examining an overlap region of AIS data and high frequency radar measurements to determine how well these two independent data sources agree. Perfect agreement between the two is unlikely based on the time periods that the measurements are made over and how the two data sources measure ocean currents.

San Francisco Harbor was selected for a comparison of AIS data and high frequency radar measurements. This location was selected due to the availability of AIS measurements and high frequency radar measurements. The AIS measurements were provided by Cloudview Photography while the high frequency radar measurements were provided by San Francisco State University. High frequency radar measurements for the total vector files were made available for an entire year. Over the 11 month period of AIS collection, over 150 million AIS messages were captured.

Due to the extensive amount of AIS data that is available, a filtering of the data was chosen to provide the best comparison between the AIS based ship drift computations and the high frequency radar data. First the AIS data was filtered down to only the high accuracy AIS position reports. These are position reports where some type of differential GNSS solution was used and so the reported latitude/longitude points are accurate to within 10 m. While no estimate is given for position reports that are not the high accuracy reports, ship drift computations could still be undertaken, but will result in larger error terms.

Next the AIS data was down selected again to ensure part of the AIS ship track would overlap with the high frequency radar measurements. The high frequency radar data provided is located inside of San Francisco Bay. Due to the positioning of the AIS receivers, ships both inside and outside of the bay are detected. This further reduced the amount of available AIS data that overlapped with the high frequency radar.

The AIS ships were also investigated to determine if they were moving. Moored ships must report their position once every three minutes. Due to the number of ships that are docked inside the bay, another subset of the AIS data is excluded from the AIS ship drift portion of the analysis. Individual ships from the remaining dataset were studied in a bit more detail to determine the trends that supported this technique and those that did not.

6.2.1 Straight Traveling Container Ship Example

One such example of a ship and how it compares to high frequency radar is the container ship depicted in figure 6.1. This ship is leaving a dock and heading out to sea. This image is of ship drift measurements from consecutive AIS measurements. The section of travel where the container ship starts traveling straight while passing Treasure Island is of interest. Figure 6.2 is a detailed image of the raw AIS computed ocean currents between consecutive AIS measurements. The white lines on the image are the high frequency radar measurements at that time. These lines are thicker at the location of the measurement and the longer line is allowed to rotate around this to depict the direction of travel of the high frequency radar measurement. This data is compared against the AIS based ocean current measurements, but an outstanding question is what should the starting and ending AIS messages be for the computation of that ocean current?

As a first attempt, the starting and ending points were selected when the ship$'$s heading became consistent to within 1^o. In this instance the ship turned to have a heading of 316^o and was within 1^o until it started turning again to have a heading of 325^o. This results in a computed ocean current of 89.1 cm/s at 190 deg. Examining what the high frequency radar states the ocean current is for the average latitude longitude combination between the starting and ending points is 50.8 cm/s at 194.6 deg. This difference of 38.3 cm/s in ocean current magnitude is larger than the error tolerances.

In an effort to get the measured ocean currents to agree more closely, some of the initial turning effects are examined. In this iteration, the first 200 seconds after the new heading is reach are eliminated from the ocean current measurement. The 200 seconds in this limit was simply chosen

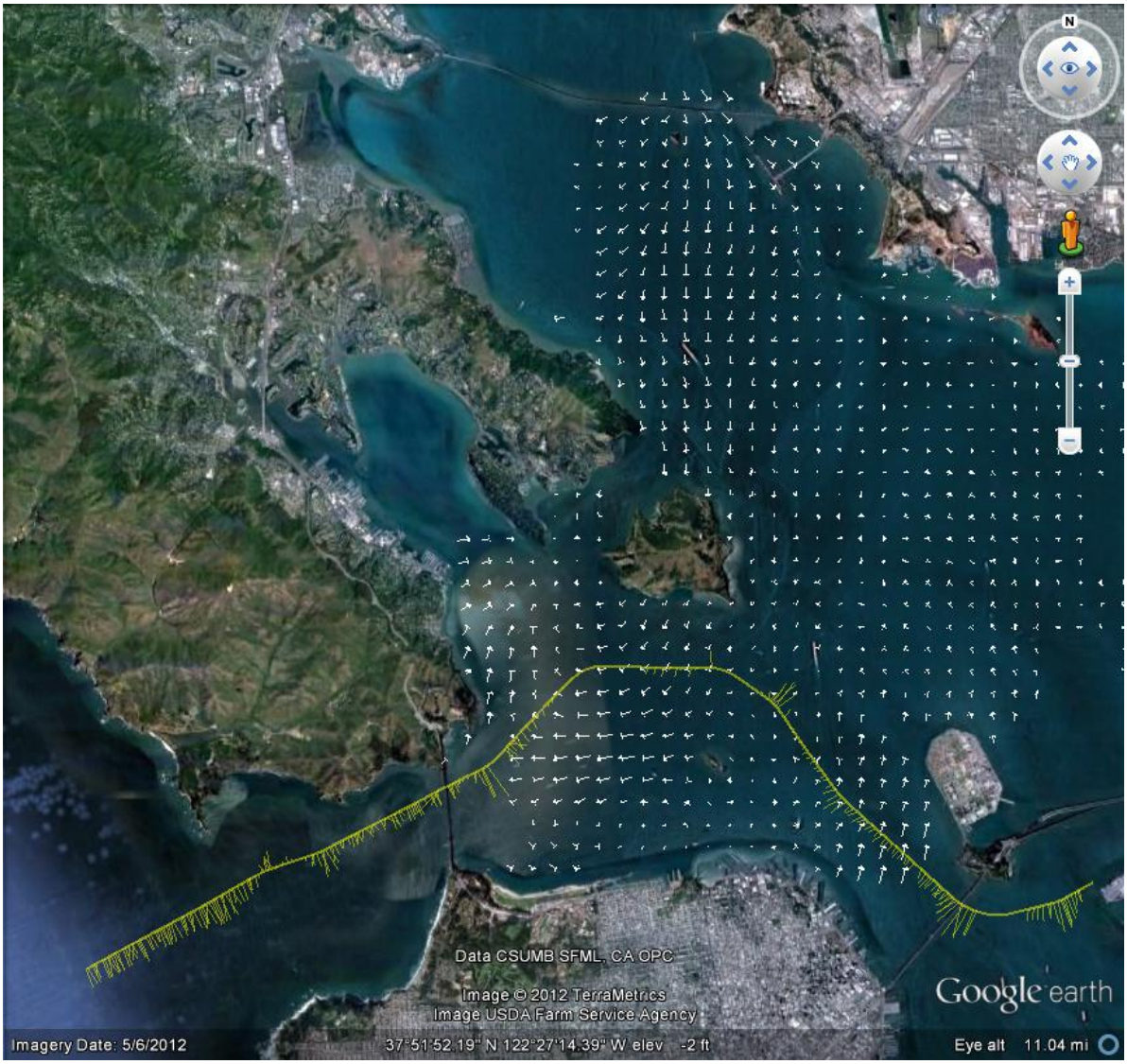

Figure 6.1: Container Ship: Raw AIS based Ship Drift Measurements

as the course over ground became more consistent from one AIS measurement to the next. When this point is chosen as the starting point, the computed ocean current from the AIS measurements becomes 45.8 cm/s at 191.6 deg. The corresponding high frequency radar measurement at the average position of the AIS measurements is an ocean current of 50.8 cm/s and 194.6 deg. This closer measurement between the AIS based ship drift and the high frequency radar measurements suggests if possible, it is desirable to eliminate the turning effects of the ship under study if possible.

The effects of the wind were also examined for this particular ship. The data for the wind was

Figure 6.2: Containter Ship: Detail Near Treasure Island

provided by datasf.org. Based on the equations and assumptions set forth in *Richardson* [1997], the average effect the wind had on this ship drift measurement was 1.2 cm/s. As this is a comparatively small amount of effect, wind effects were ignored for the rest of the dissertation.

It should also be noted that this example is an instance where the ship is traveling in a direction with 120^o between the ocean current and the ship′s heading. When there is a 90^o separation, the signal to noise ratio of the ocean current on the ship should be at a maximum. This signal to noise ratio will be a minimum when the heading and the ocean current are in the same direction or

in exact opposite directions. Also this ship does have a change in speed between the starting and final AIS measurements. Normally, the ship drift technique assumes that the ship under study is at a steady state. This also perturbs the accuracy of the AIS ship drift technique.

DeHaan [1998] states "wave effects appear to play an important role by decreasing the signal to noise ratio in regions of weak currents, making it difficult to correct the ship-drift velocities." While this references the importance of the weak vs strong current discussion, there is also the orientation of the ship with respect to the current as well. 6.3 shows another description of signal to noise where a low signal to noise would be the yellow regions, those where the ship's heading and the ocean current direction are within 45^o of each other.

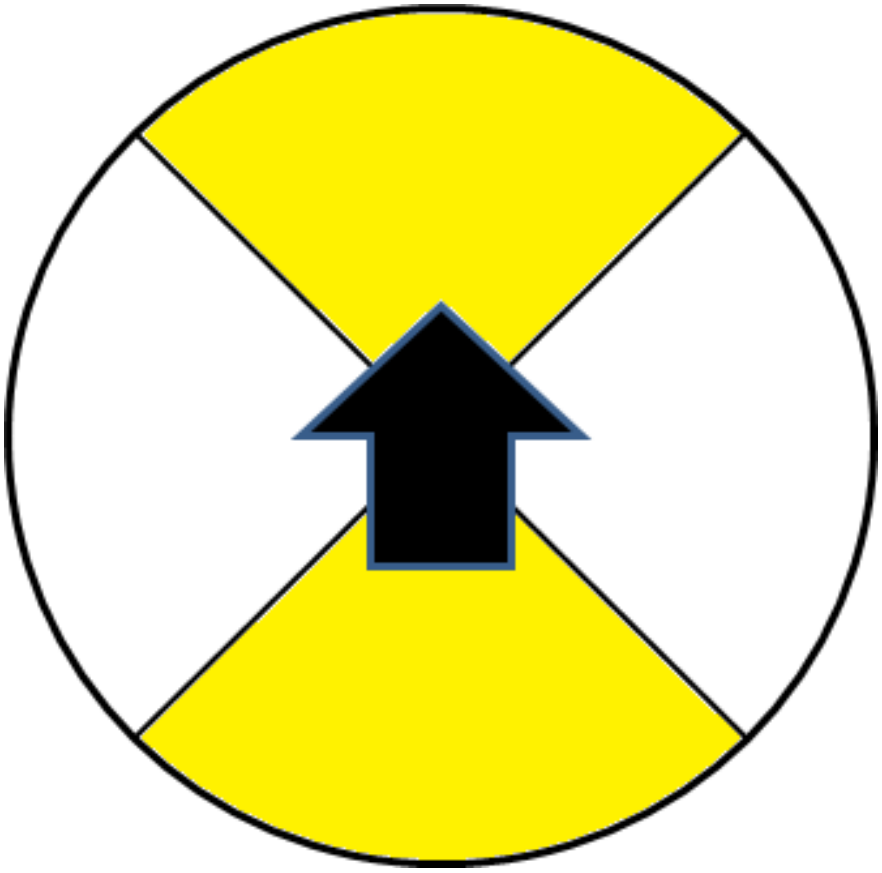

Figure 6.3: Orientation of the Ship with Respect to Ocean Current

In the following roll up case studies, the computed ocean current measurements are also examined by their residuals with respect to the angle between the ocean current direction from the

validation data source and the ship's heading to see if this broadside impact of the current improves the measurement or not.

6.2.2 Ship Traveling Into Current

As stated previously, when a ship is heading into a current or with a current, the signal to noise ratio will be at a minimum. This situation is one of the more difficult ones for a ship drift computation to be undertaken. One such example of a ship is depicted in Figure 6.4. This ship is an oil tanker that is heading into port. The section that is under investigation had a heading that was constant to within 1^o. Turning effects in this instance were ignored as they appeared to have a minimal impact as no sharp turn occurred prior to this strecth of ship track. The computed ocean current was 36.3 cm/s at 145^o. The corresponding HF radar measurement at the average location is 68.5 cm/s at 178.4^o.

Some contributions to the difference between ship drift measurements and the high frequency radar could be the ship is slowing down. In this instance, the speed over ground change is impacting the values of the computed ocean currents. By sampling at both longer and shorter time periods, the computed ocean current changed with the speed over ground. A longer sampling of the ship track leads to a computed ocean current of 113 cm/s. The large variability of the computed ocean current based on the longer or shorter ship tracks is another reason why the low SNR configuration is suspect for computing ocean current via AIS based ship drift.

6.3 Ship Drift Measurements of Colocated Ships

Another investigation of the ship drift technique involves the examination of computed ocean currents from two different ships in the same region at similar times. Just outside the bay the shipping lanes provide an opportunity to match ships by location. Figure 6.5 depicts the ship tracks of two ships in the shipping lane separated by approximately 53 minutes. These two ships computed ocean currents that were 35 cm/s at 148 deg and 71 cm/s at 164 deg. Both of these ship tracks are less than 2 minutes of time.

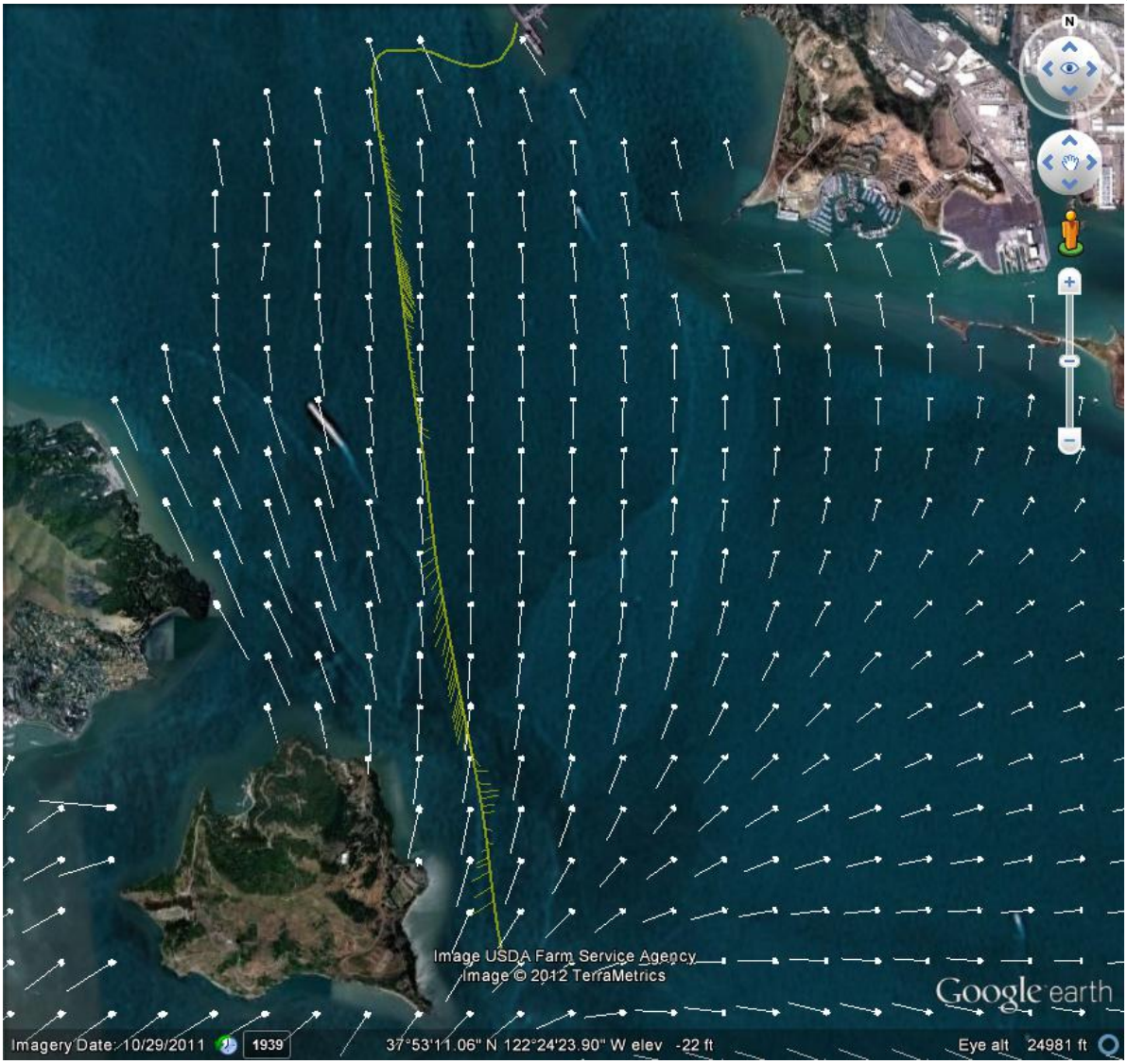

Figure 6.4: Raw Measurements of Oil Tanker Slowing Down to Down Traveling Into a Current

A different portion of the ship track was examined for both of these ships when the ships overlapped to examine how consistent the computed ocean current was. For the one ship when the 2 minute track above was expanded to 7 minutes, the computed ocean current is 35 cm/s and 110 deg. This computed ocean current is consistent in magnitude and a difference of 38 deg in direction. The other ship has a truncated time period of 26 seconds due to a turning effect and had a computed ocean current of 70 cm/s at 153 deg. Once again the magnitude is consistent and the direction is different by 11 deg. Consequently, both of these ships are consistent with

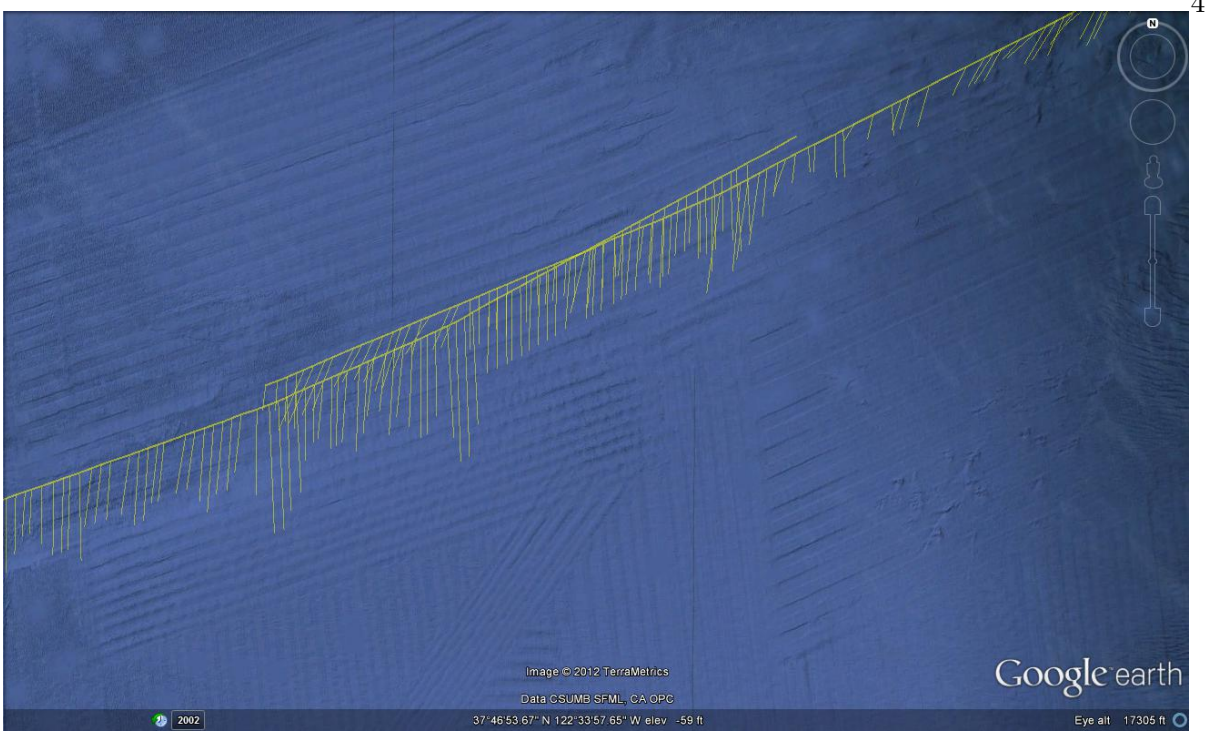

Figure 6.5: Shipping Lane Ship Overlap

themselves and the ocean current magnitude seems less sensitive to the selection of starting and ending measurements.

Based on the criteria that was determined by examining individual ships a multiple day examination of AIS based ship drift is performed. The filter was run over a 49 day period. The AIS measurement has to be consistent in heading with no more than a 1^o variation in heading. Also, the first 3 minutes of any ship track were ignored to ensure there would be no turning effects that could possibly corrupt the measurements. Once an ocean current is computed, the computed location needed to be within 500 m of a high frequency radar measurement. This 500 m criteria was selected as that is the resolution of the high frequency radar measurements.

When the above filter criteria is applied, there are 549 different AIS computed ocean currents. These estimates of ocean currents have an average ocean current magnitude of 32.2 cm/s and 81.6^o for a direction residual.

Examining the plot, there appears to be a decrease in the residuals for instances where the

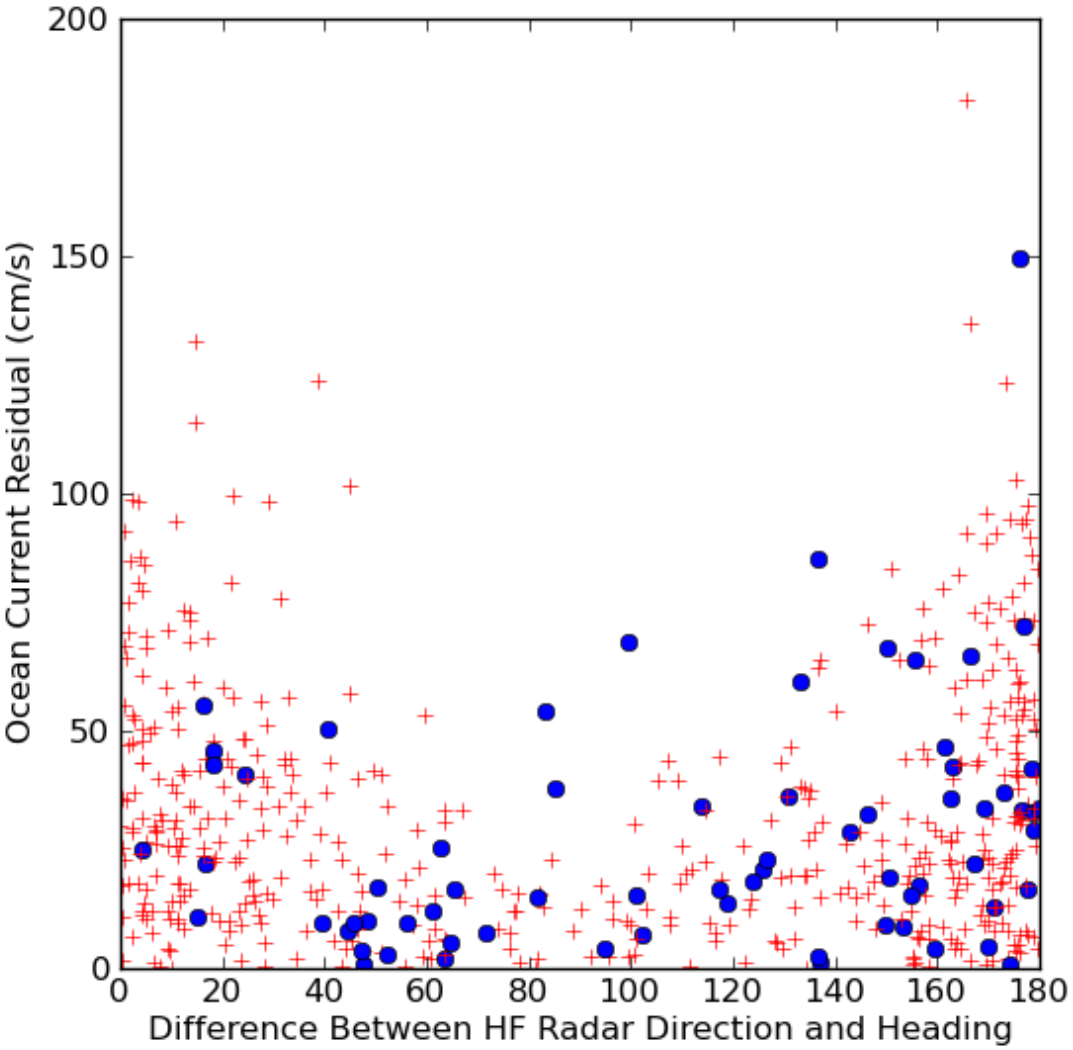

Figure 6.6: Ocean Current Magnitude Residuals

current is impacting the ship at an angle between 45^o and 135^o. The blue dots are for measurements where there was more than a 4 degree angle separation between the COG and the heading of the ship. A similar plot is created for the residual of the ocean current direction, 6.7

The metrics for how the residual numerically change is captured in table 6.1.

The table summarizes how for currents that are impacting the broadside of a ship, the ocean current residuals decrease. A similar conclusion can be drawn for measurements that have a larger

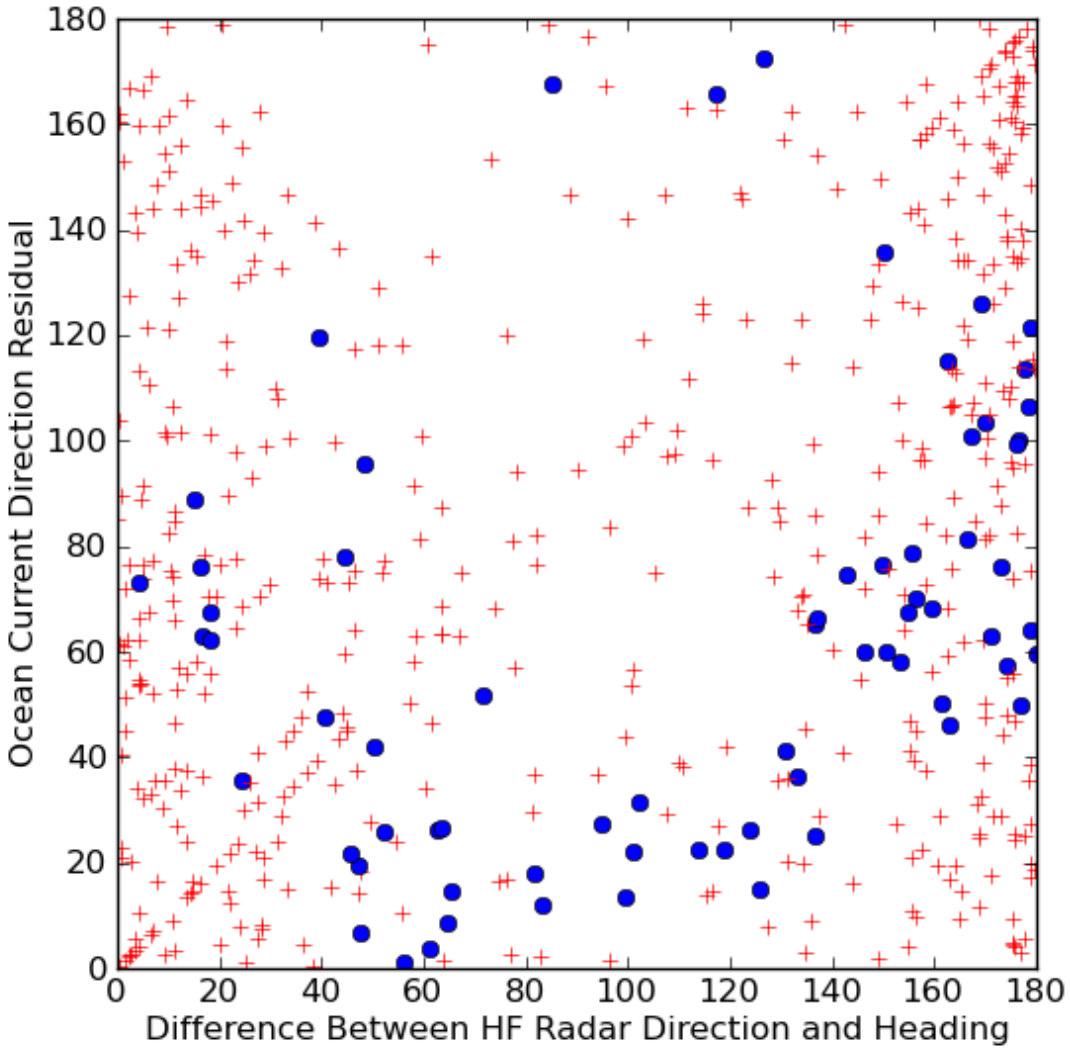

Figure 6.7: Ocean Current Direction Residuals

separation in angle between the COG and the heading. One of the drawbacks of the AIS data in San Francisco Bay is ships need to turn more frequently than in the open ocean and this produces short ship tracks. The longest ship track used was 410 seconds long (6 min 50 seconds). These short ship tracks are compared against the high frequency radar measurements which are averaged over a 50 minute time period. Open ocean AIS data should allow for longer ship tracks.

Table 6.1: San Francisco Ocean Current Residuals

Portion of Data Set	Ocean Current Magnitude (cm/s)	Ocean Current Direction (Deg)	Number of Points
All	32.2	81.6	549
Angle $< 45^o$ or Angle $> 135^o$	36.6	85.3	417
$45^o <$ Angle $< 135^o$	18.2	69.8	132
Greater than 4^o Angle Separation	26.7	57.1	56
Less than 4^o Angle Separation	32.9	84.4	493

6.4 AIS data and Ship Drift in the Gulf of Mexico

ORBCOMM was kind enough to provide some AIS data for ships traveling in the Gulf of Mexico for ocean current computations. Due to how the data is time tagged, sometimes the same AIS message was time tagged several hours apart. This difference in how the data is time tagged would result in inaccurate dead reckoning vectors that are either too long or too short and corrupt the ocean current measurement. To account for this, a quality factor parameter is considered. This quality factor is simply a ratio between the actual distance traveled and the predicted dead reckoning vector. As a first order filter, if this quality factor is between .9 and 1.1, those ocean current measurements are treated as possibly valid values based on consistent AIS measurements. The AIS measurements that are outside these limits can be caused by either a timing issue, the ship changing speed, the ship changing course and correcting back to the original heading or any combination thereof.

6.4.1 Differences Between Ship Drift Estimated Ocean Currents and Geostrophic Ocean Currents

Ship drift ocean current estimates are a combination of the ocean current acting on the hull below the waterline, the effect of the wind on the ship and wave effects. The geostrophic

currents for the validation data source are primarily derived from satellite altimetry data with measurements of sea surface height [*Leben*, 2005]. The geostrophic currents are also provided on a 0.25 latitude/longitude grid. The distance between AIS measurements varies between 2 km and almost 300 km. Based on the differences in currents being measured, the time period of them being measured and the distance averaged over for the ship drift calculations, it is expected to have some differences between the estimated ocean currents. Observing the trends of the residuals between the measurement types gives some additional insight to how the ship drift estimations are working.

For this case study, three days worth of ORBCOMM measurements were used and consisted of approximately 58,250 messages. Unfortunately, due to the amount of ships that are stationary and other ships turning, 40 AIS based ship drift ocean current computations are possible based on the filter criteria used. These 40 ocean current computations are compared against the geostrophic currents. The locations of these computations are depicted in Figure 6.8.

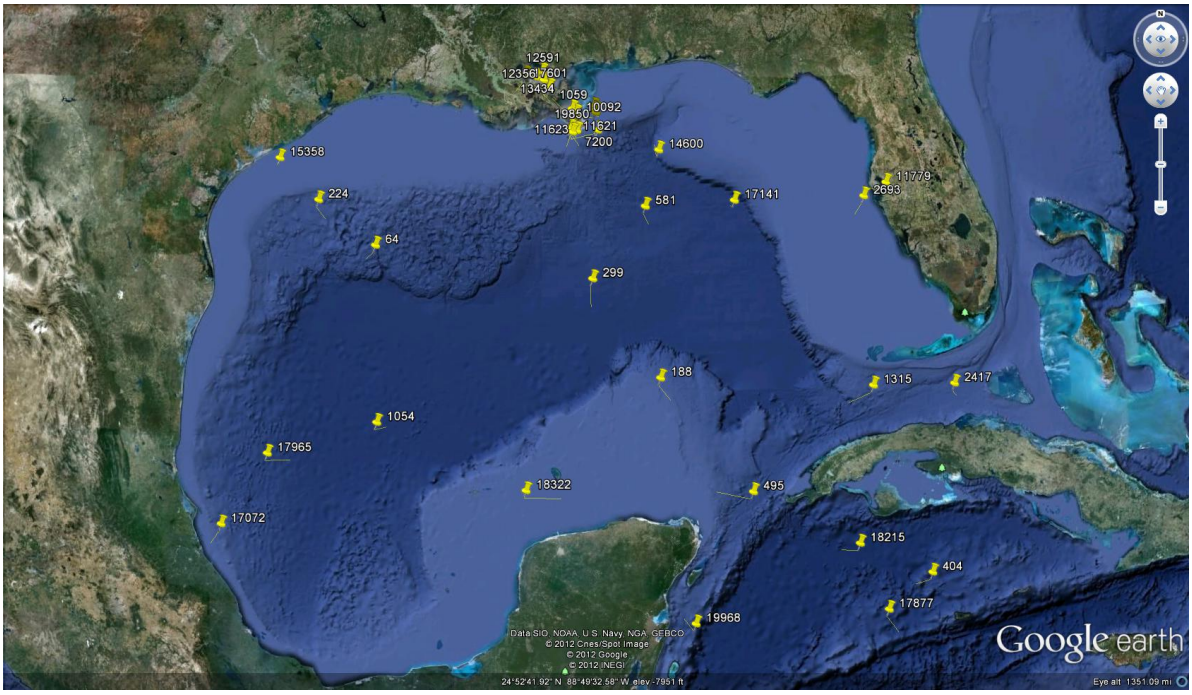

Figure 6.8: Locations of ORBCOMM Derived Ocean Currents

The residual between the ORBCOMM computed ocean currents and those from satellite altimetry had an average residual of 20.2 cm/s for a magnitude residual and 79.4 deg for a direction

residual. The filter used assumes between AIS measurements the heading does not change by 2 degrees between measurements. If the residuals are examined where there is no change in heading vs. a change in heading by 1 degree, the residuals are comparatively smaller for the computations with a consistent heading.

Table 6.2: ORBCOMM Ocean Current Residuals

Portion of Data Set	Ocean Current Magnitude (cm/s)	Ocean Current Direction (Deg)	Number of Points
All	20.2	79.4	40
Change in Heading is 0^o	18.8	73.6	16
Change in Heading is 1^o	21.2	83.2	24
Change in COG is <= 1^o	19.7	65.4	22
Change in COG is > 1^o	20.9	96.5	18
Dead Reckoning Distance < 10000m	16.2	88.2	17
Dead Reckoning Distance > 10000m	23.2	72.7	23

An examination of how the residuals change based on the variance of the course over ground between AIS measurements is performed. When there is less than a 1^o change in COG, the residual decreases. When the COG changes by more than 1^o the residuals increase. This residual change is seen mostly in the direction component. The variability of the COG measurements between AIS messages implies some level of variability of the underlying forces acting on the ship. With more consistent COG measurements, a more accurate determination of the ocean current direction can be made.

Another way to examine the residual data is by examining the distance between the AIS measurements. When the residuals are examined for distances less than 10,000 m vs. greater than 10,000 m, the improvement in ocean current magnitude and direction are no longer linked. For the shorter distances, the ocean current magnitude residual decreases. For longer distances, the ocean current direction residual decreases. This trend would exist as longer distances allow for

more time for the actual distance vector and the dead reckoning vector to separate allowing for a more accurate direction measurement. The longer distances with dead reckoning also suffer from a proportionally larger error in the dead reckoning vector than the actual distance vector. The actual distance error for longer distances gets proportionally smaller. The dead reckoning error however increases with an increase in magnitude of the dead reckoning magnitude. This helps to explain why the magnitude of the estimated ocean current is better for short distances, but not as good for the longer distances.

The geostrophic current is only one component of surface currents. The ship drift based estimates were also consistently higher than the currents computed geostrophic currents. As such, a different time period was selected to compare the ORBCOMM data against an ocean model.

6.5 ORBCOMM and the HYCOM Ocean Model

For this analysis, the 27^{th} of November was selected as it should provide more clear currents for comparison as compared to the October date. For this day, the satellite had 78626 different AIS position reports. The tidal currents were ignored for the Gulf of Mexico analysis as they are less than 8 cm/s in magnitude [*Ecology Panel Committee to Review the Outer Continental Shelf Environmental Studies Program Board on Environmental Studies and Toxicology National Research Council*, 1992]. When the filtering criteria was applied against this dataset, 87 ship drift estimates were made. When these were compared against the HYCOM model, one of the AIS computations was recommended for deletion due to the excessively large ship drift measurement that was estimated. Examining the remaining residuals show 6 more ship drift estimates that are suspect. When these 6 additional estimates were examined, they were from 3 ships all near ports in shallow water. Table 6.3 shows how the residuals are effected based on the elimination of these estimates.

A depiction of the ships where the ocean currents are estimated is shown in Figure 6.9.

Many of the reported locations are near the coastline and near ports which makes sense based on where ship traffic would be expected. Also, this dataset would be improved by having more

Table 6.3: ORBCOMM Ocean Current Residuals Against HYCOM

Portion of Data Set	Ocean Current Magnitude (cm/s)	Ocean Current Direction (Deg)	Number of Points
All	32.4	74.0	87
Unrealistic Current Eliminated	24.7	76.7	86
Large Current Near Port with Low SNR Eliminated	19.2	76.9	80

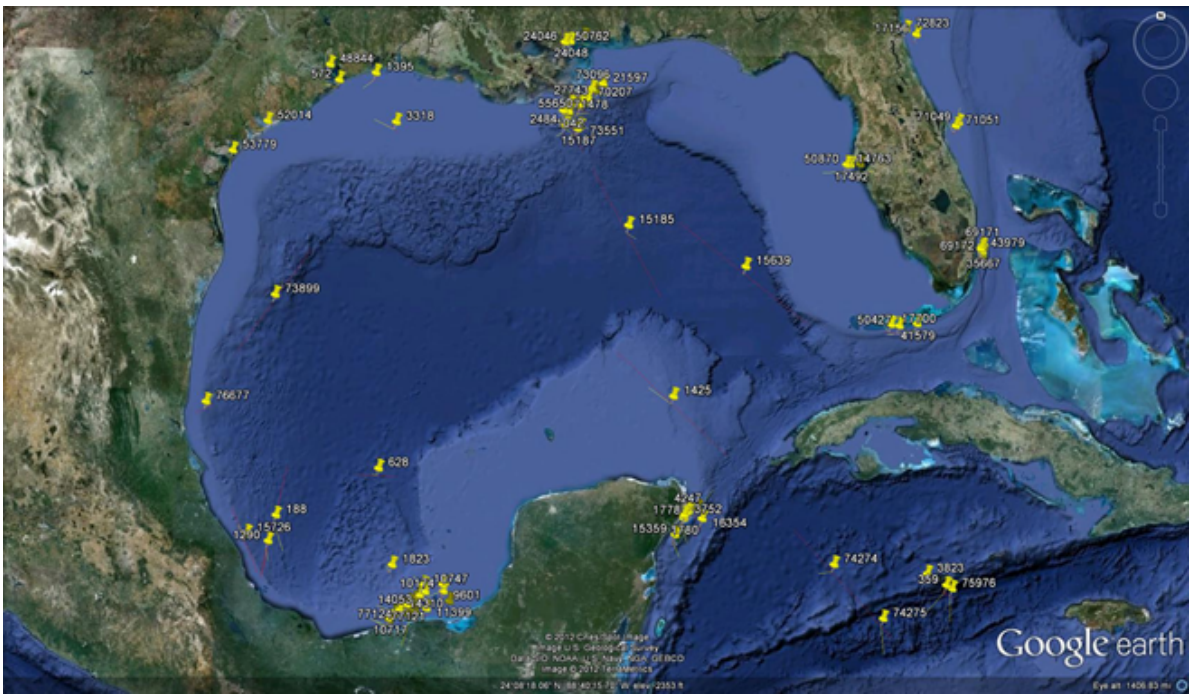

Figure 6.9: Estimates of ORBCOMM based Ship Drift Against the HYCOM Model

frequent AIS updates. Examining the subsequent messages, some of the ships are showing more speed over ground changes than those in San Francisco. This should be expected as some of these ships are traveling for upwards of 11 hours between message updates.

6.6 AIS, Moored Ships and Ocean Current Direction

Using AIS from moored ships to have a better understanding of the harbor has been discussed by both *Chang and Xinyu* [2010] and *Tadeusz et al.* [2010]. *Tadeusz et al.* [2010] in particular examined the use of AIS data to determine if a ship was "staying on anchor or drifting". While not successful, their analysis was simply a differencing in AIS positions from one measurement to the next. By examining how those AIS measurements relate to each other on a map, a more interesting signal is observed with respect to ocean current direction.

The goal of this case study is to simply determine if it is possible to help measure the direction of the ocean current using AIS data. As the mooring line will exert an additional external force on the ship, any current magnitude would be suspect without a measurement of the force on the mooring line which would not be readily available. This seems to limit AIS measurements to determining the direction of the ocean current only.

The AIS standard requires ships that are moored to report their position once every 3 minutes. For ships that are docked at a pier, the AIS transmitted location is very consistent between these 3 minute reporting intervals. Figure 6.10 is an image of how the AIS positions for a ship that was docked at a pier changed over the course of several hours. At no point did the AIS position change by more than 20 meters for the two most separated position reports. As such, there is not much useful information that can be gained from the study of docked ships other than the consistency of the GNSS position solution.

Figure 6.11 is an image of a ship′s reported position as it is leaving San Francisco Bay. When it was docked at the pier, the ship position never varied by more than 27 meters during the time at the pier. Once underway, the reported positions followed the ship track. The AIS based ship drift technique could provide ocean currents for this ship provided all the associated caveats are met.

Other ships that have their navigational status flag set to moored, have reported positions that vary more than those of the hard docked ships. One such ship that was investigated was showing the ship′s position changing almost 400 m over the duration of a day but never had

Figure 6.10: Hard Docked Moored Ship Position Over Time

a speed over ground exceed 0.1 knots. This particular ship was investigated in more detail to determine what was occuring with these particular reports. Figure 6.12 shows how this particular ship is not located at a pier.

To obtain a better understanding of the dynamics of this ship, the location of the ship was plotted and colored by time. This image is shown in Figure 6.13.

Examining the time scale, while the overall movement of the ship changes by over 300 meters, consecutive measurements appear next to each other regularly. To further help understand what is occurring with this image, a nearby current prediction at Potrero Point [*MobileGeographics*, 2012] was selected and the markers were changed to squares for periods of ebb currents and circles for periods of flood currents. Most of the time, the circles representing the flood current are South

Figure 6.11: Ship Leaving Port Position Over Time

and slightly East of the average position. The squares representing when the ebb current occurred appear mostly to the North and West of the average location. To illustrate what physically is occurring, Figure 6.14 is used.

In this image, the vertical lines represent the slack current where a flood or an ebb current later occurs. The plot shows how during periods of flood currents, the ship has a heading of approximately 330 degrees. During periods of an ebb current, this heading changes to approximately 170 degrees. This shows how the heading of the ship is changing based on the local current conditions.

To see if these results could be reproduced, a second ship was selected that was located just over 2 km away from the first ship. When that ship′s position was examined over the first day, a

Figure 6.12: Moored Ship in Middle of South Bay Position Over Time

similar rotating reported position was observed and is displayed in 6.15.

Based on the similar ship behavior, this ship was then plotted on the same image of how the heading changed with time and is shown in 6.16.

Freely rotating ships, while they are anchored, can provide a certain level of insight into the direction of the ocean current if the current direction is constant.

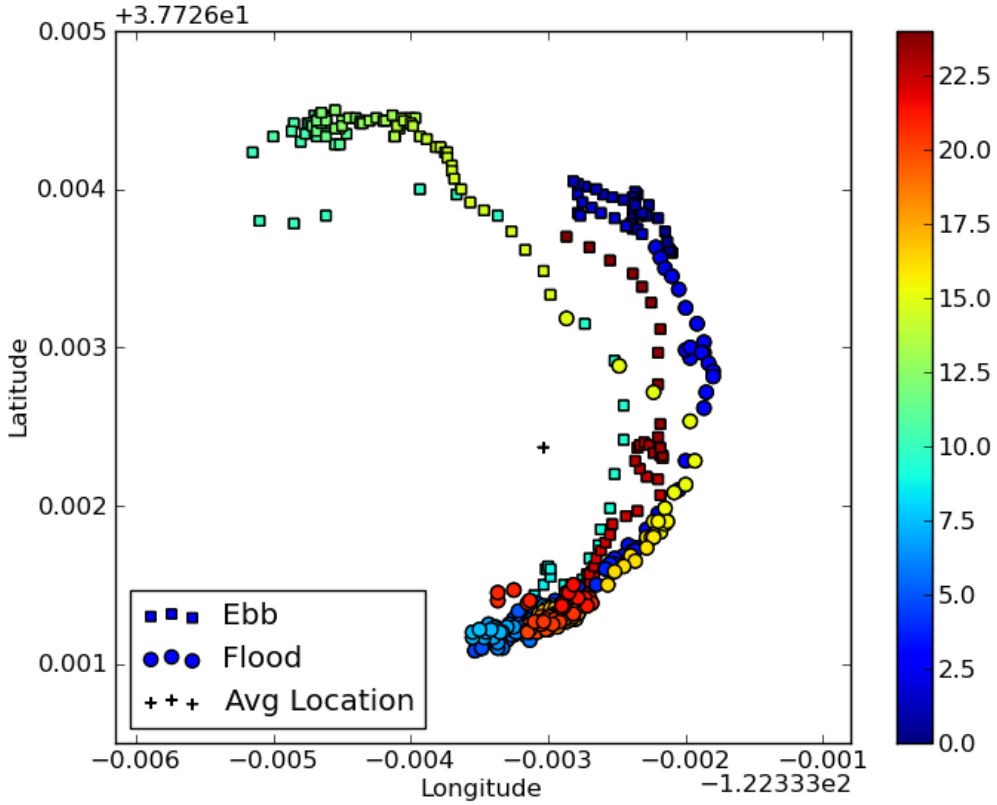

Figure 6.13: Moored Ship Position Over Time

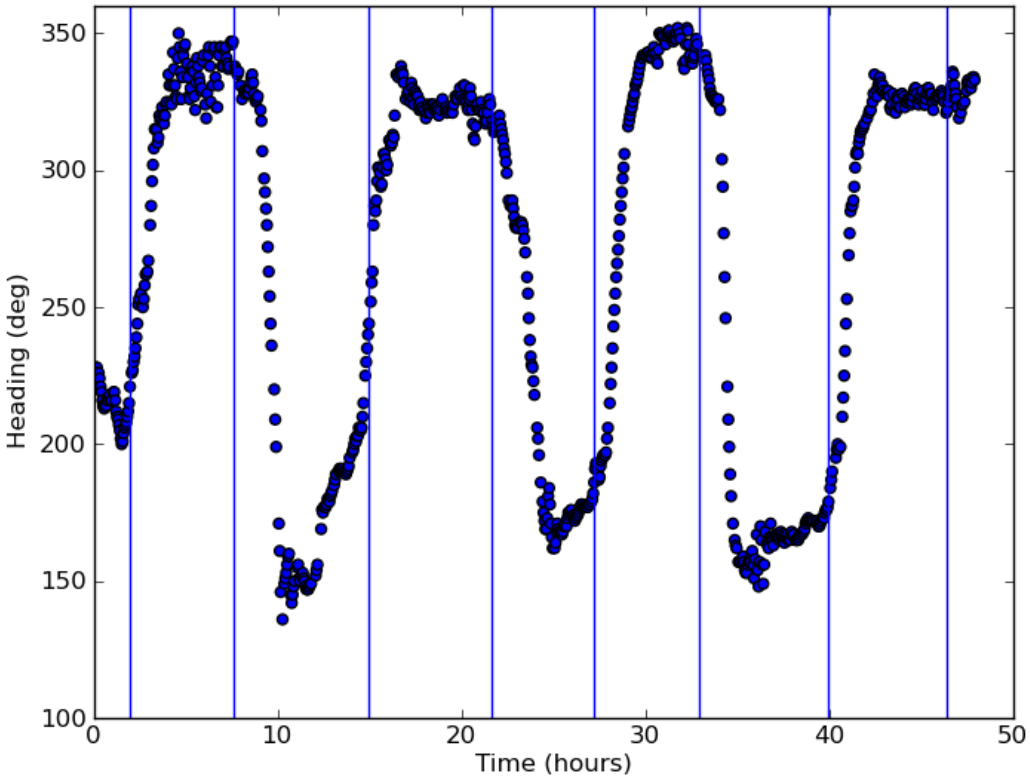

Figure 6.14: Moored Ship Heading vs Time

Figure 6.15: Second Moored Ship in Middle of South Bay Position Over Time

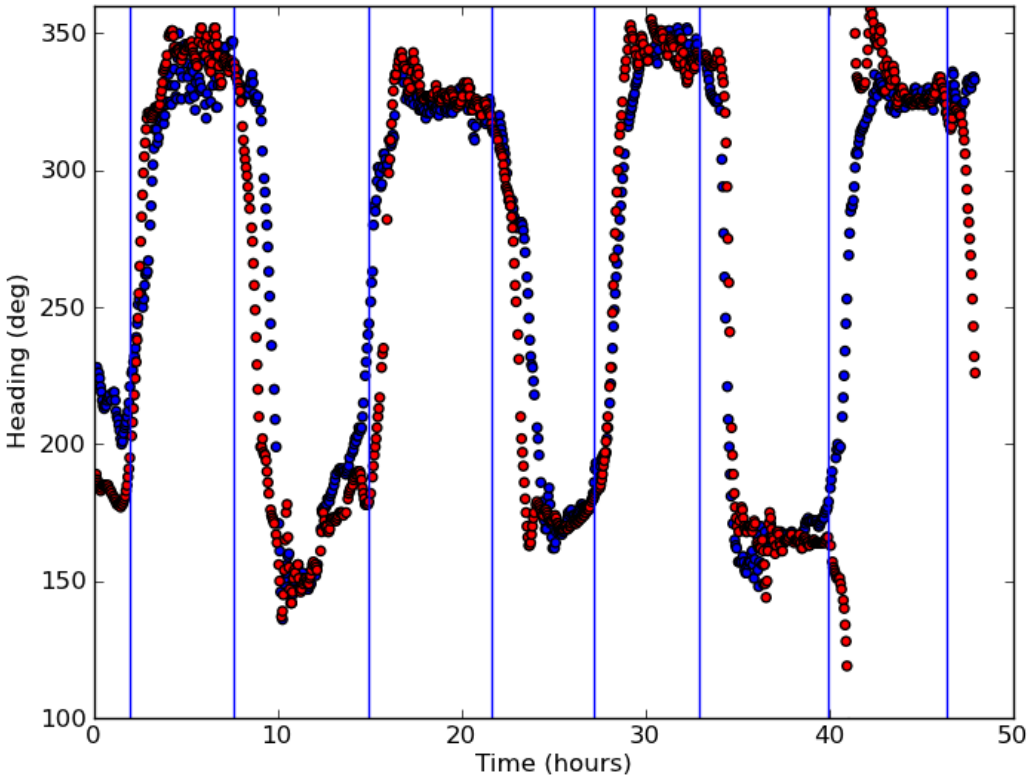

Figure 6.16: Two Moored Rotating Ships in the Middle of South Bay Heading vs. Time

Chapter 7

Conclusions

The ship drift technique benefits from the use of AIS in its solution. The more frequent AIS measurement allows for finer resolution ship drift measurements to be computed. This allows for smaller scale ocean features to be examined if the ship density covers the area of interest. The AIS provides a system to more rapidly send data to data centers than what was done previously. The ability of AIS to use GNSS allows for more precise ocean currents to be computed. Combining AIS with a satellite system like ORBCOMM, allows for global coverage of the AIS based ship drift computation to enable currents to be computed at any location where ships are present.

Upon computing ocean currents via AIS based ship drift technique several observations were made. 1) The AIS based ship drift ocean currents are more than an order of magnitude more precise than the ship drift computations that were made in *Richardson and McKee* [1984]. 2) The longer baselines between AIS measurements were shown to decrease the relative error. 3) There are conditions where the ship drift technique is less reliable than other instances. 4) The ocean current needs to be strong enough to impart a large enough force on the ship to perturb the ship track. If there is a small ocean current or the orientation of the ship is such that the ship is running with or against the current, the ship drift technique will be less reliable. A broadside current will have a larger impact on the ship and allow for a more accurate ship drift computation. 5) The separation between the heading and the course over ground is one observable that implies a stronger SNR ratio. 6) It should also be noted that faster ship speed generally improves the accuracy of the ship drift computation. 7) Longer baseline AIS based ship drift computations improve the direction

residual. 8) Some level of ocean current direction can be determined from anchored ships that are allowed to freely rotate.

One of the other areas of discovery is with working with shorter ship tracks, non-steady state effects of the ship's measurements potentially corrupt the ship drift measurements. These non-steady state effects include the turning effects of the ship and if a ship is increasing or decreasing the ship's speed.

AIS based ship drift measurements should improve the precision of the ocean current measurements in the open ocean. The AIS based ship drift measurements compared favorable with high frequency radar measurements when there was a higher SNR. Ships traveling in the same location can be compared against each other for consistency. Also, just by observing the AIS measurements, ships that are moored and allowed to freely rotate can be used to determine the direction of the ocean current. Ultimately, AIS based ship drift provides the ability to improve the quality and quantity of ocean current measurements.

Bibliography

Arnault, S. (1987), Tropical Atlantic Geostrophic Currents and Ship Drifts, *J. Geophys. Res.*, *92*(C5), 5076–5088.

Barrick, D., and W. Rector (2011), Studies of Spatial and Temporal Surface Current Turbulence Outside Golden Gate, in *Current, Waves and Turbulence Measurements (CWTM), 2011 IEEE/OES 10th*, pp. 142 –148, doi:10.1109/CWTM.2011.5759542.

Barrick, D. E., M. W. Evans, and B. L. Weber (1977), Ocean Surface Currents Mapped by Radar, *Science*, *198*(4313), 138–144, doi:10.1126/science.198.4313.138.

Calvin C Teague, J. F. V., and D. M. Fernandez (1997), HF Radar Instruments, Past to Present, *Oceanography*, *10*(2), 40–44.

Chang, L., and W. Xinyu (2010), Application of AIS in AtoN Surveillance Service, in *2010 6th International Conference on Networked Computing (INC)*, pp. 1–4.

Cheng, R. T., and J. W. Gartner (1985), Harmonic Analysis of Tides and Tidal Currents in South San Francisco Bay, California, *Estuarine, Coastal and Shelf Science*, *21*(1), 57 – 74, doi:10.1016/0272-7714(85)90006-X.

Cloudview (2009), Hi-Def San Francisco, http://hd-sf.com.

Conomos, T., R. E. Smith, and J. W. Gartner (1985), Environmental Setting of San Francisco Bay, *Hydrobiologia*, *129*, 1–12.

Davidson, F. J., A. Allen, G. B. Brassington, Ø. Breivik, P. Daniel, M. Kamachi, S. Sato, B. King, F. Lefevre, M. Sutton, and H. Kaneko (2009), Applications of GODAE Ocean Current Forecasts to Search and Rescue and Ship Routing, *Oceanography*, *22*, 176–181.

DeHaan, C. J. (1998), Correcting for the Leeway Effect on Ship-Drift Data: When Can it be Done Reliably?, Master's thesis, The Florida State University.

Deser, C., and M. L. Blackmon (1993), Surface Climate Variations Over the North Atlantic Ocean During Winter: 1900-1989., *Journal of Climate*, *6*, 1743–1753.

Ecology Panel Committee to Review the Outer Continental Shelf Environmental Studies Program Board on Environmental Studies and Toxicology National Research Council (1992), *Assessment of the U.S. Outer Continental Shelf Environmental Studies Program:II. Ecology*, The National Academies Press.

Emery, B. M., L. Washburn, and J. A. Harlan (2004), Evaluating Radial Current Measurements from CODAR High-Frequency Radars with Moored Current Meters, *Journal of Atmospheric and Oceanic Technology*, *21*, 1259.

Eriksen, T., A. Skauen, B. Narheim, O. Helleren, O. Olsen, and R. Olsen (2010), Tracking Ship Traffic with Space-Based AIS: Experience Gained in First Months of Operations, in *2010 International Waterside Security Conference (WSS)*, pp. 1–8, doi:10.1109/WSSC.2010.5730241.

Graber, H. C., D. R. Thompson, and R. E. Carande (1996), Ocean Surface Features and Currents Measured with Synthetic Aperture Radar Interferometry and HF Radar, *J. Geophys. Res.*, *101*(C11), 25,813–25,832.

Harlan, J. A. (2003), Short Time Scale Effects on High Frequency Radar-Derived Current Velocity Measurements, Ph.D. thesis, University of Colorado.

ITU-R (2010), *Technical Characteristics for an Automatic Identification System Using Time-Division Multiple Access in the VHF Maritime Mobile Band.*, International Telecommunications Union, itu-r m.1371-4 ed.

Kim, S. Y., and E. Terrill (2009), Lagrangian Applications of the Coastal Surface Currents Using High-Frequency Radar in California, in *Radar Conference, 2009 IEEE*, pp. 1–5, doi: 10.1109/RADAR.2009.4977099.

Laws, K., J. Vesecky, and J. Paduan (2011), Monitoring Coastal Vessels for Environmental Applications: Application of Kalman Filtering, in *Current, Waves and Turbulence Measurements (CWTM), 2011 IEEE/OES 10th*, pp. 39–46, doi:10.1109/CWTM.2011.5759521.

Leben, R. (2005), Altimeter-Derived Loop Current Metrics, *Geophysical Monograph - American Geophysical Union*, *161*, 181.

Leben, R. R., G. H. Born, and B. R. Engebreth (2002), Operational Altimeter Data Processing for Mesoscale Monitoring, *Marine Geodesy*, *25*(1-2), 3–18, doi:10.1080/014904102753516697.

McPhaden, M. J., D. V. Hansen, and P. L. Richardson (1991), A Comparison of Ship Drift, Drifting Buoy, and Current Meter Mooring Velocities in the Pacific South Equatorial Current, *J. Geophys. Res.*, *96*(C1), 775–781.

MobileGeographics (2012), Potrero Point 1.1 mi E, South San Francisco Bay, California Current Requested time: 2009-04-03 12:00 AM PDT, http://tides.mobilegeographics.com/locations/5077.html?y=2009&m=4&d=3.

NOAA (2013), Tides & Currents (Golden Gate Bridge), http://tidesandcurrents.noaa.gov/.

Ohlmann, C., P. White, L. Washburn, B. Emery, E. Terrill, and M. Otero (2007), Interpretation of Coastal HF Radar-Derived Surface Currents with High-Resolution Drifter Data, *Journal of Atmospheric and Oceanic Technology*, *24*(4), 666–680.

ORBCOMM (2012), AIS, http://www.orbcomm.com/services-ais.htm.

Paduan, J. D., K. C. Kim, M. S. Cook, and F. P. Chavez (2006), Calibration and Validation of Direction-Finding High-Frequency Radar Ocean Surface Current Observations, *IEEE Journal of Oceanic Engineering*, *31*(4), 862 – 875.

Peterson, D. H., T. Conomos, W. W. Broenkow, and P. C. Doherty (1975), Location of the Non-Tidal Current Null Zone in Northern San Francisco Bay, *Estuarine and Coastal Marine Science*, *3*(1), 1 – 11, doi:10.1016/0302-3524(75)90002-X.

Pickard, G., and W. Emery (1990), *Descriptive Physical Oceanography An Introduction*, 5th ed., Butterworth Heinemann, Oxford.

Pond, S., and G. Pickard (2003), *Introductory Dynamical Oceanography*, 2 ed., Butterworth Heinemann.

Richardson, P. (1985), Drifting Derelicts in the North Atlantic 1883-1902, *Progress In Oceanography*, *14*(0), 463 – 483, doi:10.1016/0079-6611(85)90023-0.

Richardson, P. (1997), Drifting in the Wind: Leeway Error in Shipdrift Data, *Deep Sea Research I*, *44*, 1877–1903.

Richardson, P. L. (1989), Worldwide Ship Drift Distributions Identify Missing Data, *J. Geophys. Res.*, *94*(C5), 6169–6176.

Richardson, P. L., and T. K. McKee (1984), Average Seasonal Variation of the Atlantic Equatorial Currents from Historical Ship Drifts, *J. Phys. Oceanogr.*, *14*(7), 1226–1238.

Sinnott, R. W. (1984), Virtues of the Haversine, *Sky and Telescope*, *68*, 158.

Stewart, R. H., and J. W. Joy (1974), HF Radio Measurements of Surface Currents, *Deep Sea Research*, *21*, 1039–1049.

Sturges, W. (1993), The Annual Cycle of the Western Boundary Current in the Gulf of Mexico, *J. Geophys. Res.*, *98*(C10), 18,053–18,068.

Tadeusz, S., W. Ryszard, and P. Sławomir (2010), Fusion of Data Received FM-CW Radar and AIS: Analysis of Functionality: Topic 3. Radar Application, in *2010 11th International Radar Symposium (IRS)*, pp. 1–3.

Taylor, J. R. (1997), *An Introduction to Error Analysis*, 2nd ed., University Science Books.

Tetreault, B. J. (2002), Use of the Automatic Identification System (AIS) for Maritime Domain Awareness (MDA), *Proceedings of OCEANS 2005 MTSIEEE*, pp. 1–5.

Vesecky, J., K. Laws, and J. Paduan (2009), Using HF Surface Wave Radar and the Ship Automatic Identification System (AIS) to Monitor Coastal Vessels, in *Geoscience and Remote Sensing Symposium, 2009 IEEE International, IGARSS 2009*, vol. 3, pp. III–761 –III–764, doi: 10.1109/IGARSS.2009.5417876.

Vesecky, J., K. Laws, and J. Paduan (2010), A System Trade Model for the Monitoring of Coastal Vessels Using HF Surface Wave Radar and Ship Automatic Identification Systems (AIS), in *2010 IEEE International Geoscience and Remote Sensing Symposium (IGARSS)*, pp. 3414–3417, doi: 10.1109/IGARSS.2010.5650279.

Wyrtki, K., L. Magaard, and J. Hager (1976), Eddy Energy in the Oceans, *J. Geophys. Res.*, *81*(15), 2641–2646, doi:10.1029/JC081i015p02641.